Theses and Dissertations (ETD)   College of Graduate Health Sciences

5-2013

Bone Properties of Recombinant Inbred Line - BXD Mouse

Yueying Angela Zhang
University of Tennessee Health Science Center

Recommended Citation

Bone Properties of Recombinant Inbred Line - BXD Mouse

Abstract

Osteoporosis is identified by reduced bone mass, decreased bone quality and altered bone micro-architecture. These traits are quantitative and also highly regulated by genetic and environmental factors. As a powerful tool for collaborative analysis of quantitative traits and gene function, BXD recombinant inbred (RI) lines mice have been used to identify genetic effects for bone density.

For the first time, we investigated the bone properties of BXD RI mice by analyzing femur and tibia and compared their phenotypes of different compartments. In this study, microcomputed tomography (μCT) provided an accurate measurement on characterizing bone quality and bone architecture ex-vivo; three-point bending provided a measurement on characterizing genetic-influence based bone structural response.

51 BXD RI mouse strains were analyzed, including progenitor C57BL/6J (n=16) and DBA/2J (n=15), and two first filial generations (D2B6F1 and B6D2F1). Bones were collected from 10 to 14-week old females and males (N≥3 each group) and bone parameters were measured at three different sites by high resolution 3D micro-computed tomography: whole bone, cortical bone (mid-shaft of femur and tibia), and trabecular bone (distal femoral and proximal tibial metaphyses).Statistical analysis was performed with SAS 9.3. Differences of each compartment between BXD RI strains were first analyzed using Mixed Effects models, where each strain was considered to be independent clusters and measurements of mouse from each strain were considered to be repeated measurements. The model results were adjusted for gender and age effects. Correlations between femur and tibia were examined using graphical statistics and Spearman's rank correlation coefficient.

Strain differences were observed in bone quality and structural properties (p

We conclude that a) femur-tibia association in bone morphological properties significantly vary from strain to strain, which may be caused by genetic differences among strains; b) strain-wise variations were seen in bone mass, bone morphology, bone microarchitecture along with bone structural property.

Document Type
Thesis

Degree Name
Master of Science (MS)

Program
Biomedical Engineering and Imaging

Research Advisor
Weikuan Gu, Ph.D.

Keywords
BXD recombinant inbred mouse, femur, tibia, morphology, structural property

Subject Categories
Analytical, Diagnostic and Therapeutic Techniques and Equipment | Investigative Techniques | Medicine and Health Sciences | Other Analytical, Diagnostic and Therapeutic Techniques and Equipment

Comments

Two year embargo expired May 2015

Bone Properties of Recombinant Inbred Line – BXD Mouse

A Thesis
Presented for
The Graduate Studies Council
The University of Tennessee
Health Science Center

In Partial Fulfillment
Of the Requirements for the Degree
Master of Science
In the Joint Graduate Program in Biomedical Engineering and Imaging
From The University of Tennessee
and
The University of Memphis

By
Yueying Angela Zhang
May 2013

ACKNOWLEDGEMENTS

ABSTRACT

Osteoporosis is identified by reduced bone mass, decreased bone quality and altered bone micro-architecture. These traits are quantitative and also highly regulated by genetic and environmental factors. As a powerful tool for collaborative analysis of quantitative traits and gene function, BXD recombinant inbred (RI) lines mice have been used to identify genetic effects for bone density.

For the first time, we investigated the bone properties of BXD RI mice by analyzing femur and tibia and compared their phenotypes of different compartments. In this study, micro-computed tomography (μCT) provided an accurate measurement on characterizing bone quality and bone architecture ex-vivo; three-point bending provided a measurement on characterizing genetic-influence based bone structural response.

51 BXD RI mouse strains were analyzed, including progenitor C57BL/6J (n=16) and DBA/2J (n=15), and two first filial generations (D2B6F1 and B6D2F1). Bones were collected from 10 to 14-week old females and males (N≥3 each group) and bone parameters were measured at three different sites by high resolution 3D micro-computed tomography: whole bone, cortical bone (mid-shaft of femur and tibia), and trabecular bone (distal femoral and proximal tibial metaphyses).Statistical analysis was performed with SAS 9.3. Differences of each compartment between BXD RI strains were first analyzed using Mixed Effects models, where each strain was considered to be independent clusters and measurements of mouse from each strain were considered to be repeated measurements. The model results were adjusted for gender and age effects. Correlations between femur and tibia were examined using graphical statistics and Spearman's rank correlation coefficient.

Strain differences were observed in bone quality and structural properties ($p<0.05$) in each bone profile (whole bone, cortical bone, or trabecular bone). Additionally, strains differences were revealed in bone stiffness ($p<0.0001$). It is well-known that skeletal phenotypes are largely affected by genetic determinants and genders, such as bone mineral density (BMD). While genetics and gender appear expectedly as the major determinants of bone mass and structure, significant correlations were also observed between femur and tibia. More importantly, positive and negative femur-tibia associations indicated that genetic makeup had an influence on skeletal integrity. For example, BXD75 presented a negative femur-tibia correlation in whole bone BMD ($r=-0.86$, $p=0.01$) while positive associations were revealed in BXD1 ($r=1.0$, $p<0.0001$) and BXD95 ($r=0.9$, $p=0.04$).

We conclude that a) femur-tibia association in bone morphological properties significantly vary from strain to strain, which may be caused by genetic differences among strains; b) strain-wise variations were seen in bone mass, bone morphology, bone micro-architecture along with bone structural property.

TABLE OF CONTENTS

LIST OF TABLES

LIST OF FIGURES

LIST OF ABBREVIATIONS

µA	Micro ampere
µCT	Micro-computed tomography
App. Dens	Apparent density (mg/cm^3)
BS	Bone surface (mm^2)
BV/TV	Bone volume density, or bone volume ratio
Conn. Dens.	Connectivity density
CSA	Cross-sectional area (mm^2)
Ct	Cortical
Ct. Ar	Cross-sectional area of cortical bone (mm^2)
Ct. mBMD	Material bone mineral density of cortical bone (mg/cm^3)
Ct. Th	Cortical thickness (mm)
DA	Degree of anisotropy
DXA	Dual energy x-ray absorptiometry
keV	Kiloelectron volt. 1 keV=1.6E-6 J
mBMD	Material bone mineral density (mg/cm^3)
MIL	Mean intercept length
Min.Vol	Mineralized volume (mm^3)
ms	millisecond
QTL	Quantitative trait loci
RI	Recombinant inbred
SMI	Structural Model Index
SNP	Single nucleotide polymorphism

Tb. N	Trabecular number
Tb. Sp	Trabecular space
Tb. Th	Trabecular thickness
Trab	Trabecular
TV	Total volume
VOI	Volume of interest
3D	Three dimensional

CHAPTER 1.   INTRODUCTION

Osteoporosis, Bone Quality and Genetic Factor

Osteoporosis is recognized as the most common bone disease in the world. It is characterized with a reduction in bone mass and an alternation of bone micro-architecture, which have been approved to be the major determinants of bone strength. A high risk of bone fragility and fracture has been observed in subjects with this bone disease.

Osteoporosis is a progressive disease which can take up to years in the development process. Therefore, accumulation of data on drug or treatment effect can take years. The incidence of femoral fractures excluding the hip has been found to be 37.1 per 100,000 persons per year and the incidence of tibial fractures (e.g. tibia, fibula, and ankle fractures) has exceeded 490,000 per year in the United States (Arneson, Melton, & Lewallen, 1988; Praemer, Furner, & Rice, 1992). As the most common long bone fractures, it is clinical important to diagnose or foresee femoral and tibial fractures. The predictability of skeletal system from one bone for another has not been addressed in bone mineral research.

Patients have osteoporosis are likely to have bone fractures in vertebrae, distal arm or femoral neck, and risk of fracture at many other sites is also increased when bone density is reduced and bone structures are deteriorated, such as tibia. Osteoporosis-related fractures have become an increasing problem in aging men and women, although the risk is greater in women than in men (Kanis, Melton, Christiansen, Johnston, & Khaltaev, 1994). Family and twin studies have shown that genetic factors play an essential role in bone mass regulation (Pocock et al., 1987; Cummings, Nevitt, & Browner, 1995). Accordingly, there has been intense bone research on genetic influence in the past few decades. Studies show that osteoporosis is highly heritable and influenced by environmental factors, such as lifestyles (Krall & Dawson-Hughes, 1993). Smoking and drinking has an influence on it as well (Laitinen & Valimaki, 1991; Kiel et al., 1996).

Animal Models

Animal models have been widely used in biomedical research, particularly for osteoporosis study. Osteoporosis is a slowly progressive disease and the response of the therapy can take up years to show results. The accumulation of data on human being is time consuming and maintenance of a study group is made more difficult due to either relocation or death.

In addition, lifestyle and health-related factors have been linked with an increased incidence of the osteoporosis, such as smoking, alcoholism and diet. For human beings, it is difficult to create a homogeneous study group without high variance

(Twyman, 2002). Therefore, it is critical to limit the number of elements influencing study results.

Animal models solve the problem by providing a uniform experimental population, such as genetically identical inbred strains. A carefully chosen, appropriate experimental animal model for the study of osteoporosis minimizes that limitations associated with studying the disease in humans, namely time and behavioral variability among test subjects. Other advantages of using rodent models are numerous. They are inexpensive, easy to house, and the general public is accustomed to the role of rodents for use in research. The recombinant inbred (RI) mouse is for manipulation of the genome and BXD mouse model is most powerful for quantitative trait loci identification. Also, the biological and biomechanical characteristics of orthopedic implants, bone-graft substitutes can be tested on large numbers of animals maintained with a level of experimental control, impossible in human clinical research. Rodent model has become the most commonly used animal model on osteoporosis.

However, some may argue that rodents rely on four legs to walk while humans walk upright. Human's bipedalism results in most body weight being carried by lower limbs while mechanical load on mouse legs is shared between fore- and hind-limbs. Therefore, it is not meaningful to compare the absolute value between human and rodent skeletal properties. On the other hand, as a genetic experimental model, mouse outperforms other animal models. Its genome is approximately the same size with human being and it contains the same number of genes showing extensive synteny (conserved gene order). In addition, most human genes have counterparts and the functions of these genes are closely related (Twyman, 2002).

Recombinant Inbred Mouse

Recombinant inbred (RI) strains were created by intercrossing two inbred lines (often classical lines) and then breeding them to homozygosity through more than 20 generations of sibling mating (**Figure 1-1**), meaning mating brothers and sisters from the same strain. The consequent genomes are homozygous and also contain a variety of genetic segments from the two parental strains. Homozygosity refers to the state of having two identical alleles of the same gene. By being homozygous, it means the genes in the subject have either two dominant alleles or two recessive alleles. This trait enables genetic mapping and linkage analysis to identify a specific loci or locus for an individual phenotype.

This experimental approach on mouse breeding had become widely accepted in studying phenotypic variations and their underlying genetic differences. In addition, this technique had enabled the repetition of the phenotypic measurements and a renewable resource of identical experimental subjects (Wade & Daly, 2005).

RI strains provided a valuable replicable nature that experiments could be arranged at different time and location. This immortalized population allowed the
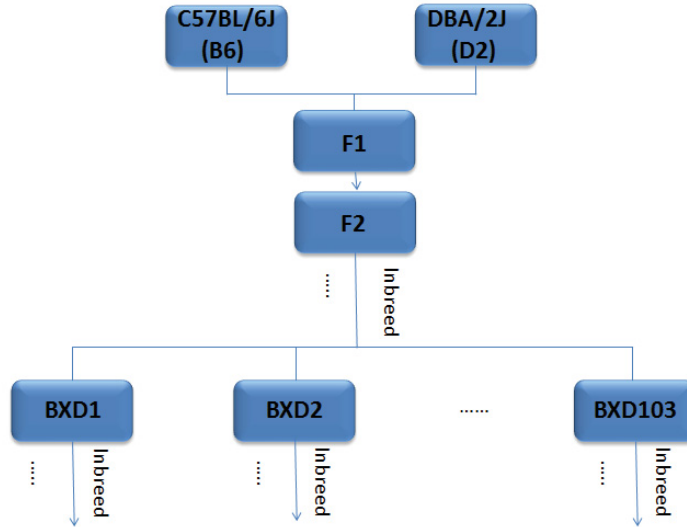
Figure 1-1.   Generation of BXD recombinant strains.
The first generation is inbred by crossing B6 and D2. F2 generation is generated by
intercross F1. Mating of brothers and sisters of F2 for more than 20 generations
produces homozygosity.

researchers to phenotype as many animals per genome as desired over extended period of time (Peirce, Lu, Gu, Silver, & Williams, 2004).

In this study, we categorized the mice into two groups based on their breeding: parental strains (C57BL/6J, DBA/2J) and offspring (D2B6F1, B6D2, and BXD). C57BL/6J was also known as B6 and DBA/2J was known as D2. These two strains were amongst the most widely and commonly used mouse strains (e.g. A/J, C3H/HeJ) and often referred as classical inbred. These two strains had homozygous genomes.

BXD Recombinant Inbred (RI) Strains

For this project, we took the advantages of uniqueness and the importance of mouse RI strain population available at UTHSC in Dr. Robert Williams' lab. With those RI strains, we will be able to obtain reliable data by duplication of experiment on the multiple mice under the same genetic background that eliminates the influence of environment and experimental errors. The results can lead to QTL (quantitative trait loci) identification with unique effects on specific phenotypes or with pleiotropic effects on multiple phenotypes.

BXD RI strains were derived by intercrossing B6 and D2. The resulting F1 generation was inbred to produce F2 and subsequent generations. Then brother and sister pairs in F5 were used to produce offspring BXD strains by inbreeding over 20 generations to ensure that BXD strains were all homozygous (**Figure 1-1**). Some BXD strains became distinct and thus not were included in the study (e.g. BXD47, BXD58, BXD72, etc.) (Peirce et al., 2004).

BXD RI strains had been well characterized for a remarkable variety of phenotype data, including drug/alcohol addiction*. A wide variety of BXD phenotype data had been collected over the past decade. However, there is a lack of information regarding the skeletal characteristics of the BXD mice.

The collection of data included the gene expression profiles from a total of 18 tissues including major tissue such as brain, liver, kidney, lung, spleen, eye, cartilage, hippocampus, cerebellum, striatum and neocortex and prefrontal cortex (Arneson et al.,1988; Airey, Lu, & Williams, 2001; Lu, Airey, & Williams, 2001; Chesler et al., 2005; Gaglani, Lu, Williams, & Rosen, 2009; Suwanwela et al., 2011). In addition, it included a variety of phenotype data from metabolism to drug addiction, from visual system to gastrointestinal system*. William's group has systematically generated quantitative data for 140 standardized phenotypes, including glucose response, body weight change, physical activity and oxygen consumption across a large subset of the BXD family by using adult males and females. These essential baseline clinical phenotypes are widely variable, often highly heritable, and in many cases can be linked

*Detailed information can be achieved on the GeneNetwork page: www.genenetwork.org.

4

to genetic loci encompassing known and novel candidate genes. Our study validates the variability among strains to help further identify genetic determinants on skeletal traits.

As a wider scope of the BXD phenotype characterization, this project would allow further investigation on neuro- skeletal interaction, and interaction between skeletal and other organ since a variety of phenotype data has been available. Eventually, the phenotyping of BXD strains could lead to a whole body systemic analysis with this tremendous pool of records.

However, the most prominent advantage of using experimental mouse was to ensure the elimination of environmental factors, e.g. food intake, lighting, physical activity, room temperature, etc. Differences observed in phenotypes would be speculated to have been resulted from genetic differences.

Mouse Age

Laboratory mice have an average lifespan of approximately 2 years, and mice aged 18-24 months are considered "old". Studies of mice in their first year of life indicate that bone structure develops rapidly from 0-2 months, while peak measures of bone mineral density and cortical size are attained by 3-6 months. Glatt et al. reported that trabecular bone volume peaks near 2 months in C57BL/6J mice, followed by decreases throughout life for both females and males (Willingham et al., 2011). Mice used in this study age from 9.6 weeks to 13.6 weeks, approximately equivalent to human age of 25 to 30 years.

Over the age of 9 weeks, mice generally had completed most of their growth and the bone formation and resorption processes that shape the bone were still active. The bone development during mouse' adulthood had not been clearly defined and needed further study. Femur length grows rapidly from week 4 to 12, after which longitudinal growth appears to cease (Ferguson, Ayers, Bateman, & Simske, 2003). Generally, a mouse would be in puberty at the age of 8 weeks and reached its adulthood at the age of 12 weeks. Particularly for RI mouse, it was reported that young mice underwent a rapid period of bone mineral acquisition and began to plateau by the age of 80-90 days (Klein, Mitchell, Phillips, Belknap, & Orwoll, 1998). Age-dependent osteoporosis did not occur until the week of 24.

High-resolution μCT

μCT, also known as micro-computed tomography, is a nondestructive technique to image bone in three dimensions. As the name indicates, it has a similar working principle with commonly used CT, but with a smaller scale and a higher resolution. μCT is typically used in research on small objects, such as small animal bones.

μCT can be seen as a 3D microscopy, which is used to examine fine-scale internal structure of objects in a three dimensional view. Additional advantages of using μCT are time- saving on sample preparation, staining, and slicing. Meanwhile, μCT preserves the complete structure of the objects. One aspect of retaining objects' full structures is to investigate the anisotropic properties of bone due to varying micro-architecture of bone in multiple directions.

μCT uses a micro-focus x-ray source to illuminate the objects and uses x-ray detectors to collect magnified projection images. Based on hundreds of views acquired from different angles by rotating the object, the computer stacks the collected cross-sectional images together to reconstruct a 3D model. The bones were not affected by radiation and no extensive sample preparation was required prior to scanning. After scanning, each bone could be used for additional examination (Postnov, Vinogradov, Dyck, Saveliev, & Clerck, 2003).

In the past, structural properties of trabecular bone have been investigated by examination of two dimensional sections of cancellous bone biopsies. Three dimensional morphometric parameters are then derived from two dimensional images using stereological methods (Parfitt, 1987). While parameters like relative bone volume (BV/TV) and surface density (BS/BV) can directly be obtained from two dimensional images, a range of important parameters such as trabecular thickness (Tb. Th), trabecular separation (Tb. Sp), and trabecular number (Tb. N) are to be derived indirectly assuming a fixed structural model, typically an ideal plate or rod model is used. Such assumptions are, however, critical due to a well-known fact that trabecular bone continuously changes its structure type as a result of remodeling. A deviation from the assumed model will lead to an unpredictable error of the indirectly derived parameters. In this study, we used metric and also non-metric parameters entirely based on direct three-dimensional calculations. The definitions and methods used for the calculation of the model independent parameters have been developed and introduced for the microstructural evaluation in Muller and Ruegsegger's study (1997).

The measurement of cancellous bone was usually taken from the secondary spongiosa where less bone turnover took place than primary spongiosa. Spongiosa referred to the spongy content of the bone. In secondary spongiosa, we observed more networks of trabeculae than the primary spongiosa.

There were several fundamental parameters that were used to derive morphological properties of bones. They were density, bone volume (e.g. total volume and VOI), and bone surface (BS).

Based on previously published work, we hypothesized that bone structures would largely vary across strains. Although some studies on investigation of the relationships between femoral and tibial properties have been done, the predictability between long bones is still not clear. Particularly, the influences of many genetic and environmental factors are not clearly addressed. In additional to the exploration in strain-wise differences in bone phenotypes, we aimed at investigating the relationship

between femur and tibia. Our second hypothesis was that, if genetic control impacted on femur-tibia correlation, a variety of associations could be revealed across strains.

There are quite a few quantitative measurements to characterize the bone structure. This list is very important conceptually since the indices will be repeated in result analysis as well as the discussion section. They have been used considerably in published studies and they will continue to stress the significance of bone mineral research. The indices and abbreviations used in this project are explained as follows.

- mBMD: Material bone mineral density.
- Min.Vol: Mineralized volume. It was the total amount of calcified content of the bone.
- BS: Bone surface. It was determined by triangulating the surface of a voxel image and calculating the total area of the triangles.
- TV: Total volume. It was the volume of the whole examined sample.
- BV/TV: Bone volume fraction or bone volume density. This normalized index was used to compare samples with different volume of interest (VOI) which was defined by a contour.
- Ct. Th: Cortical thickness. CSA: Cross-sectional area.
- Ct. Ar: Cross-sectional area of cortical bone.
- Trab BV/TV: Trabecular bone volume density.
- Conn. Den: Connectivity density. It was the number of connected structures in a network calculated based on Euler characteristics of Odgaard and Gundersen (1993). The cancellous bone connectivity had been hypothesized to be one of the primary reasons for decreasing strength and stiffness in osteoporosis.
- SMI: Structural model index. It was calculated based on 3D image analysis of triangulated bone surface with a value ranging from 0 to 3, depending on the volume ratio of rods and plates with 0 as being ideal plate and 3 as being ideal cylindrical rod structure. For a structure with both plates and rods of equal thickness, the value is between 0 and 3 depending on the volume ratio between rods and plates (Hilderbrand, Laib, Muller, Dequeker, & Ruegsegger, 1999). This index was used to quantify the characteristic shape of a three-dimensionally described structure. This quantification method had been employed to characterize the cancellous bone as "plate-like" or "rod-like". In addition, it was an independent measurement from volume, surface area, thickness and connectivity density. This index could be potentially used to assess the bone remodeling due to aging (Hilderbrand & Ruegsegger, 1997).
- Tb. Th: Trabecular thickness. It was determined by filling maximal spheres into the space between bone structures using distance transformation. The value was given by the mean thickness of all bone structures. This direct approach was derived independently on assumed model and therefore, not biased by deviations of the actual structures from this model. The method provided a measurement on mean local thickness and the thickness distribution of 3D objects (Hilderbrand & Ruegsegger, 1997).
- Tb. N: Trabecular number. It was the inverse of the mean distance between mid-axes of the structure to be examined (**Equation 1-1**). The mid-axes of the

structure were assessed from the binary 3D image using 3D distance transformation and extracting the center points of non-redundant spheres which filled the structure completely (Shenzhen Better Industrial Co. Ltd., 2012). Therefore, the measurement values of BS/TV were discarded from the analysis.

$$\boldsymbol{Tb}.\ \boldsymbol{N} = \frac{1}{2} * \frac{BS}{TV} = \frac{1}{Tb.\ Sp + Tb.\ Th}$$ **(Equation 1-1)**

- Tb. Sp: Trabecular space. It was the separation between trabecular structures. This parameter could be used to quantify the space of cavities and bone marrow. The actual distance in the 3D space was calculated by filling maximal spheres in the non-bone parts of the dimensional image, which was the same principal with thickness calculation. The size, shape, distance, and connectivity of trabecular elements impacted on biomechanical properties of the cancellous bone, and they reflected bone remodeling activity.
- DA: Degree of anisotropy. It was an architectural index to indicate the geometrical anisotropy of a structure. It was defined as the ratio between the maximal and minimal radius of the mean intercept length (MIL) ellipsoid (Toulouse, 1998). This index measured the orientation of trabecular elements using mean intercept length (MIL) (Shenzhen Better Industrial Co. Ltd., 2012). The directional MIL is the total length of the test lines in one direction divided by the number of intersections with the bone-marrow interface of the test lines in the same direction. The MIL distribution is calculated by superimposing parallel test lines in different directions on the 3D image (Hilderbrand et al., 1999). It is a measure of how highly oriented substructures are within a volume of trabeculae since trabecular orientation varies largely due to mechanical loading.

Three-point Bending

Bending tests have been useful on deriving mechanical properties of bone samples. Three-point and four-point bending tests, torsion test, tensile and compressive tests were usually available. However, for small animals, it was difficult to apply tensile or compressive test. For mouse femurs, usually 12 mm long with approximately 7 mm of diaphysis, it would be infeasible to apply four-point bending tests although it produced pure bending between the two upper loading points ensuring transverse shear stresses to be zero. Another reason for the negation on four-bending test was unequal force applied at each loading point. The test required equal forces which could only be achieved in regular shaped specimens where the condition was violated using whole bones, asymmetrical shaped specimens (Cowin, 2001).

Therefore, we chose three-point bending test to measure the mechanical properties of long bones. The advantage of three-point bending loading is the simplicity regardless of the high shear stresses created near the mid-section of the bone. In bending tests, specimens would be loaded with force until failure.

Stiffness was measured during the test. Bending caused tensile stresses on one side of the bone and compressive stresses on the other. Bone was weaker in tension than compression which was due to compliance with loading. Accordingly, cracks were usually seen on the tensile side of the bone first (Cowin, 2001).

CHAPTER 2.   LITERATURE REVIEW

Mouse has long been used for scientific research and inbred strains of mice have been used extensively to study the genetic influence on phenotypes, such as behaviors and organ functions. The benefit of using inbred strains of mice was that it provided a plethora of genomically identical mice (Twyman et al., 2002).

Quantitative trait refers to continuous characters such as height, weight and density. This BXD strain set is the largest mouse RI mapping panel to date. It includes 46 recently generated strains at Dr. Williams's laboratory (Peirce et al., 2004) and 36 previously generated strains from the Jackson laboratory (Taylor et al., 1999). All of those mice were derived from C57BL/6J (B6) intercrossing DBA/2J (D2).

Unlike classic inbred strains, the genotype of BXD strains was somewhat limited to only two alleles at each locus, passed down from the progenitors, B6 and D2. This feature allows combining the hundreds of available genomic markers for each strain and the publicly accessible databases for rapid linkage studies and for determining map distances. This step could be achieved using as few as 1 or 2 mice phenotyped from each BXD strain. To establish genetic linkage, the phenotypes could be used to obtain a strain distribution pattern to be compared with the strain distribution patterns of the known polymorphic loci previously established in the BXD strain set. When congruence between strain distribution patterns was found, linkage of the phenotype of a specific chromosomal region could be established. Up to date, all the available BXD strains had been genotyped at exceedingly high density (625,000 SNPs). Also, both parental strains had been well sequenced (e.g. DBA/2J by our group at UTHSC using SOLiD systems). Approximately 1.8 million SNPs (www.genenetwork.org) had been characterized between two parental strains. This provided unprecedented power in screening candidate genes.

Another reason for characterizing BXD bone properties was to prepare for future systematical analysis. BXD RI strains had been profiled on gene expression for a total of 18 tissues, such as liver, cartilage, hippocampus, cerebellum, and neocortex (Arneson et al., 1988; Airey et al., 2001; Lu et al., 2001; Chesler et al., 2005; Gaglani et al., 2009; Suwanwela et al., 2011).

Recent work in mouse models gives strong evidence that bone mass, bone structure and strength are regulated by an identifiable set of genes. In Klein's study, 12 chromosomes were identified for whole body BMD in 18 BXD strains. They also claimed the age influence on peak whole body BMD around 80 to 90 days where accrual rate of bone mineral acquisition plateaus (Klein et al., 1998). However, bone mineral measurement DXA (dual energy x-ray absorptiometry) is susceptible to small size of subjects which possess little surface area. Without taking the depth of material into consideration, the method itself is problematic than volumetric bone mineral density measurement. Gender-specificity was reported in Klein's study in 2001 where similar technology was employed.

Other significant train-wise differences in total and cortical density were reported in femur by Beamer et al. in 1996 (Beamer, Donahue, Rosen, & Baylink, 1996). They were using peripheral Quantitative Computed Tomography, abbreviated as pQCT, to measure the bone density. In 2000, it was reported that cortical thickness and mid-shaft stiffness in femur was influenced by genetic factors in Turner et al. study, using inbred strains B6 and C3H (Turner et al., 2000). Femoral length has been investigated by identifying associated genetic loci while tibial length was found to be genetically different among inbred mice (Akhter et al., 2000; Drake et al., 2001). In addition, genetic factors have been identified for cross-sectional area (including bone and marrow space enclosed by periosteum) (Klein, 2002). Cortical (compact bone) area in both femur and tibia were addressed as genetically influenced in C3H/HeJ, C57BL/6J and DBA2J (Akhter et al., 2000). However, in these studies, only a limited number of inbred strains of mice are shown.

For trabecular bone profile, significant differences of bone volume fraction, trabecular number and space between inbred mice were observed in lumbar vertebra (Akhter et al., 2000). Genetic influences were found in bone volume ratio along with connectivity density, trabecular thickness, SMI in femur of C57BL/6J (n=8), C3H/HeJ (n=8), and Balb/cByJ (n=9) (Bower et al., 2006). Trabecular number and trabecular spacing were confirmed with signciant difference between C3H and B6, or D2 by histomorphometry in Akhter's study (Akhter et al., 2000). However, material bone mineral density and degree of anisotropy had not been investigated for genetic influence. Degree of anisotropy provided information about how highly trabeculae align with one another which is indicative of the orientation of loading in physiological state.

For structural properties of femur, stiffness had been documented as significantly different between C57BL/6J and C3H/HeJ, 157±3 and 258±3 respectively (Turner et al., 2006).

In previous studies, most of the bone features (both morphological and mechanical) had been examined regarding their association with genetic influence except for mineralized volume. This parameter had been a useful index in histology. Therefore, it has been included this parameter in the measurement and analysis to accomplish bone profiling for BXD strains.

Furthermore, no study had been conducted for the genetic influence on the bone development association between femur and tibia. The predictability of long bones is not clear. If positive correlation could be found between femur and tibia, clinical diagnosis could be provided to either of the bone based on bone property assessment of the other. On the other hand, if there is negative or no correlation found between femur and tibia, it would be a pitfall to assume similar bone properties these two types of long bones. Additionally, it would be interesting to discover any potential influences from genetic factors on this association. Therefore, we investigated properties of tibia along with femur.

From another perspective of the bone mineral research, materials have been an important part of the experimental design. In previous studies, it has been limited to classic inbred strains, e.g. C57BL/6J and DBA/2J, where few successes for genes contributing to complex, multigenic traits have been achieved. An important problem has been the lack of resolution in identifying the causal gene(s) from the results of a linkage study (Twyman, 2002). This problem is addressed using the Hybrid Mouse Diversity Panel (HMDP), including 100 commercially available inbred strains consisting of 29 classic inbred strains and three sets of recombinant inbred strains. This panel of mouse provides sufficient power to map traits that contribute 10% of the overall variance. Importantly, the resolution of the panel is an order of magnitude better than linkage analysis (Twyman, 2002).

CHAPTER 3. METHODOLOGY

Animals

All mice used in the experiments were sacrificed using a protocol approved by the Memphis Veterans Affairs (VA) Medical Center (**Appendix A**). Strict breeding environment provides a means to circumvent complicating environmental factors. These mice were originally obtained from the Center for Neuroscience Department of Anatomy and Neurobiology University of Tennessee Health Science Center (855 Monroe Avenue Memphis, Tennessee). The male and female mice were from two progenitor strains C57BL/6J (n=16), DBA/2J (n=15) and we phenotyped 47 BXD recombinant inbred (RI) strains (from 9.57 to 13.57 weeks' old). There were 46 BXD recombinant inbred strains that had sufficient number of animals (n≥3 for each strain) for testing. There were 41 strains with male and female animals, 5 strains only with males, and 1 strain only with females. D2B6F1 (n=9) were derived from an intercross of the progenitor strains (female DBA/2J and male C57BL/6) and B6D2F1 (n=7) were derived from a cross between female C57BL/6 and male DBA/2J. In total, 358 mice were collected for sacrifice. For our project, the distribution of age for mice used on this project is presented with respect to gender in **Figure 3-1**.

After all, one femora and one tibiae were collected free of soft tissue observed by naked eyes from each mouse. A total of 696 mice long bones were collected (355 femurs and 341 tibias) and 611 of them were included in the study (337 femurs and 274 tibias) to ensure a sufficient number of samples (n≥3) for each strain. Bones were harvested postmortem and cleared off of the surrounding connective tissue as could be seen by eyes for contrast enhancement in µCT and energy expenditure reduction in mechanical test. The femoral heads and necks are retained on the femurs, while the fibulas were removed from tibia.

Specimens Handling

Bone specimens underwent X-ray imaging and mechanical testing was required to be preserved and stored with special care. Ethanol preserves protein (bone marrow), bone mineralization and hydration. In this study, 70% ethanol was used to preserve bone specimens for best morphological examination (maintaining protein structure) whereas formalin could be best use for bone histology.

High-resolution µCT

In order to quantitatively assess the structural changes with genetic variation, morphometric and architectural indices were determined from the micro- tomographic examinations. In this study, high-resolution micro-computed tomography (µCT40;
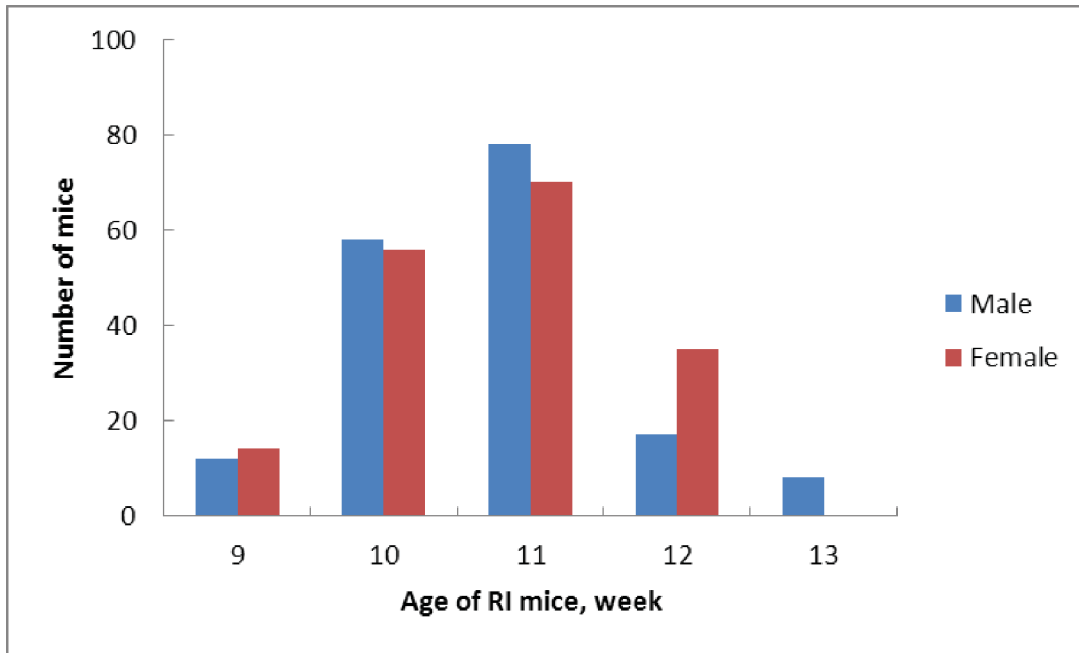
Figure 3-1.   Distribution of age for RI mice used on this project.
Blue represents male and red represents female. There is relatively equal number of
mouse in the range of 9 to 11 week. For mice at the age of 12-week, there is larger
number of female than male mice while a few male mice at the age of 13-week were
used.

Scanco Medical, Basserdorf, Switzerland) was used to scan and characterize the bone profile regionally,which was presented by the morphometric indices computed on three bone levels of femur and tibia: whole bone, cortical bone in diaphysis and trabecular bone in metaphysis. The bone samples were placed in a 12.3-mm-diameter sample holder in 70% ethanol and immobilized with plastic foams. The samples were scanned at 8-μm resolution. Morphometric and architectural parameters of bones were assessed and realistic 3D visual models were constructed for the object by selecting the volumes of interest (VOI).Data were acquired at an energy level of 55 keV, with 2000 projections, an integration time 300 ms, and an intensity of 109 μA. 3D trabecular parameters were evaluated using a fixed Gaussian filter and a thresholding of 220 for cancelous bone and 250 for cortical envelope.

Whole Bone Analysis

For whole bone analysis, three parameters were measured: length, mineralized volume, and material bone mineral density. Material bone mineral density (mBMD), sometimes engineers referred it to tissue mineral density (TMD), as a comparison to bone mineral density (BMD).

The length of femur was measured consistently from the connection of femoral neck and greater trochanter (**Figure 3-2A**) to the connection of four condyles at the distal end (**Figure 3-2B**), while the length of tibia was measured from the tibial plateau (**Figure 3-2C**) to the distal tibia denoted by the separation of fibula and tibia which can be seen in **Figure 3-2D**. This measurement was representative of the length of bone shaft as shown in the **Figure 3-3**. Mineralized volume measured the total mineral capacity of the entire specimen. Material bone mineral density measures the volumetric density of calcium hydroxyapatite (CaHA) averaged in the whole sample.

Cortical Bone Analysis

For cortical bone analysis, a cross-sectional region of 100 transverse slices (a total length of 0.8 mm) at the middle of the bone was acquired (**Figure 3-4**). For each measurement point acquired at the same settings as the trabecular site, cortical area (Ct. Ar.), cross-sectional or total area (CSA), marrow area (Ma. Ar), cortical thickness (Ct. Th.) were evaluated with the same Gaussian filter on a 0.5-mm region (50 slices). Area moment of inertia (I_{min} and I_{max}) were evaluated on the same region.

Cancellous Bone Analysis

For trabecular bone analysis, a region of 100 transverse slices at the secondary spongiosa in distal femur or distal tibia site was measured (**Figure 3-4**). The bone volume fraction was calculated directly by plotting gray voxels representing bone
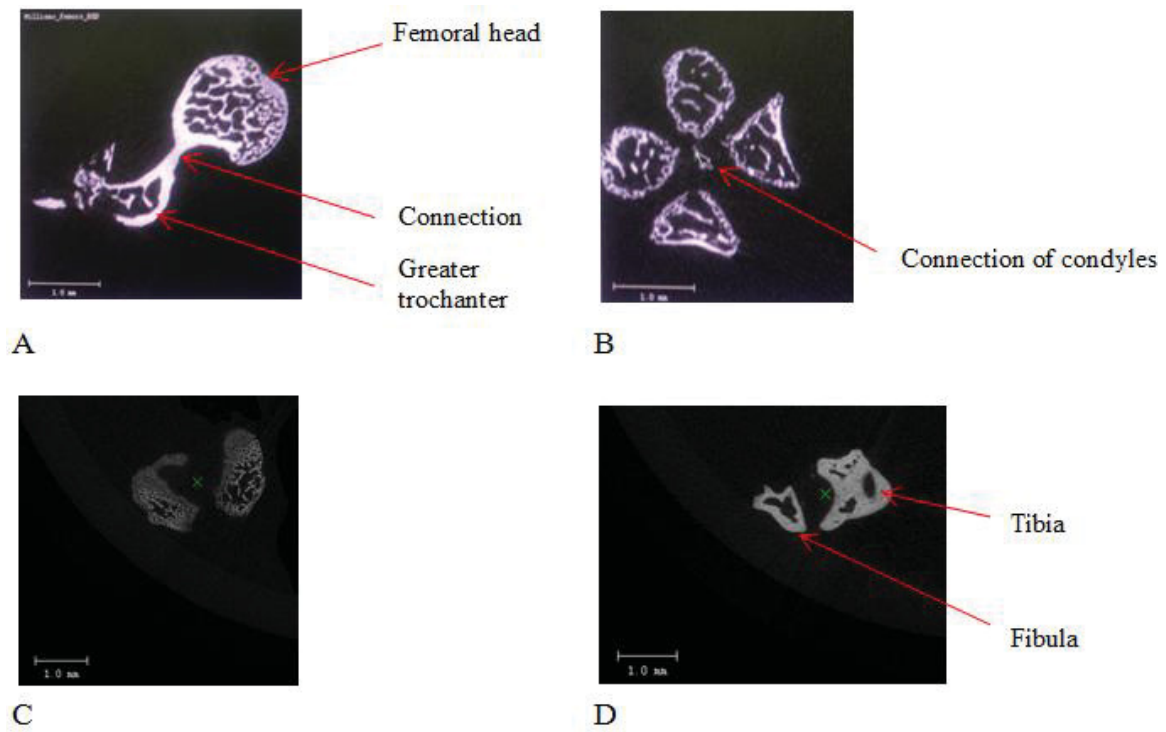
Figure 3-2.   The μCT scans illustrating the beginning and end of the length measurement.
A) The femoral-neck-trochanter junction; B) The connections of condyles at distal femur; C) tibial plateau; D) the separation of tibia and fibula.
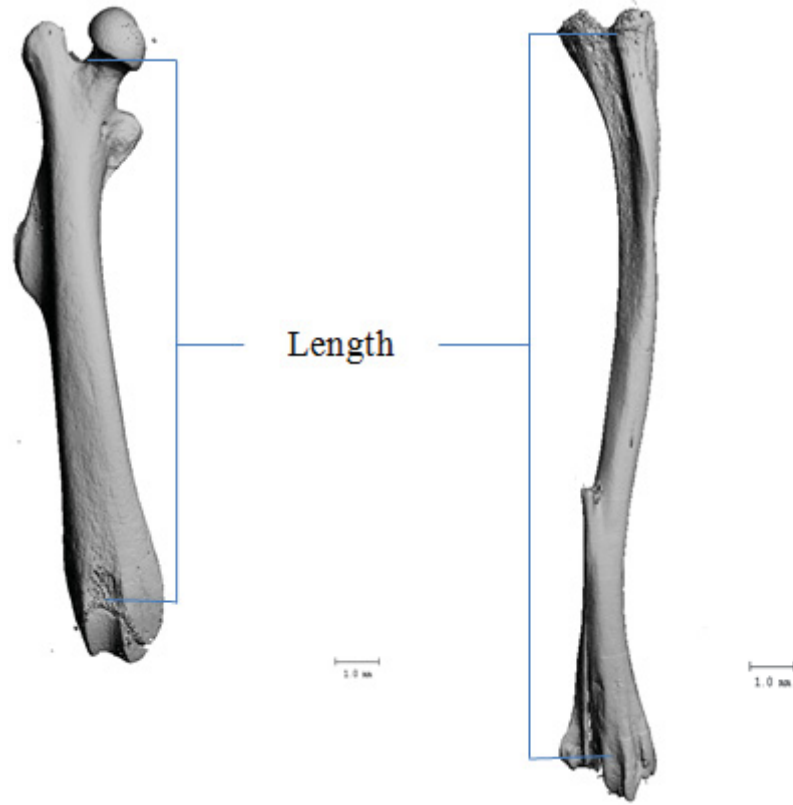
Length

Figure 3-3. **Schematic of length measurement on RI mice femur and tibia.**
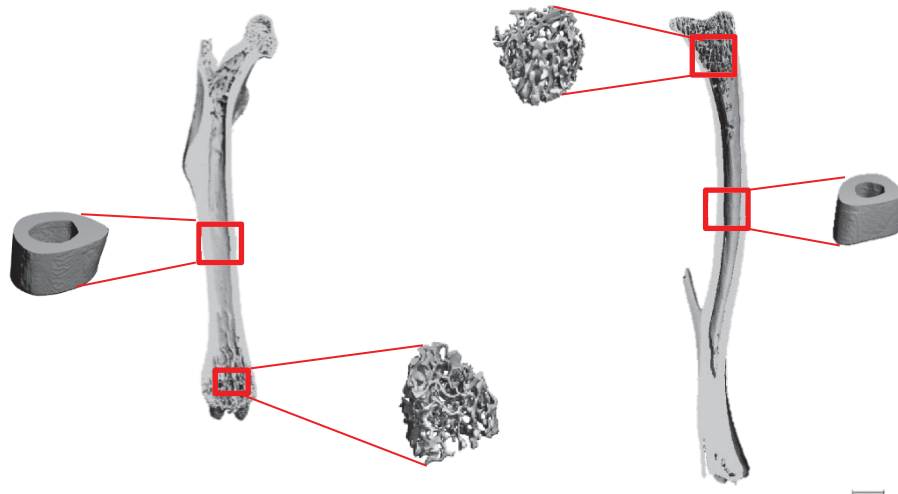
Figure 3-4. **The approximate location of 100 µCT cross-sectional scans of femur (on the left) and tibia (on the right) in RI mice.**
Cortical measurements were taken at mid-shaft while trabecular measurements were taken at distal femur or proximal tibia.

fraction against gray plus black voxel (non-bone objects; VOX BV/TV). Bone surface (BS) was calculated using a tetrahedron meshing technique generated by the "marching cubes method" and total volume (TV) was taken the volume of interest (VOI). The normalized indices (BV/TV, BS/BV, and BS/BV) were used (Martin, David, Vico, & Thomas, 2008).

3D metric indices were calculated using direct techniques based on the distance transformation, without assuming a constant model. Direct indices Tb. Th, Tb. Sp, Tb. N, were calculated following distant transformation method.

The plate-rod characteristic of the structure was estimated by the structure model index (SMI). The geometric degree of anisotropy (DA) is defined as the ratio between the maximal and minimal radius of the MIL ellipsoid. Connectivity density (Conn. Dens.) was calculated using the Euler method of Odgard and Gundersen (Martin et al., 2008).

Three-point Bending

All femoral specimens were loaded to three-point bending for mechanical property testing (**Figure 3-5**). The testing machine (Instron, Norwood, MA) was used located in Room 301A at the University of Memphis, maintained at a room temperature of 24°C. The fulcrums (0.5 mm of radius) were set to 6mm apart. The span width (6mm) was selected to secure the uniform cylindrical beam shape of the material between fulcrums, in another word, to circumvent fulcrums.

The supports were positioned equidistant from the load application site. The equipment had a force resolution of 0.05N and the crosshead speed during testing was 0.2mm/s. and force-displacement data was collected every 0.01s. Preload was often used to remove any slack in a specimen or any load recording resulted from rotation of the specimen at the testing. Therefore, a preload of 0.5 N was set for the program to discard any data during pre-load. From the data, a force versus displacement graph was created and the stiffness (S; N/mm), and Young's Modulus (E; GPa) were calculated. Load magnitude and displacement data were collected by the Bluehill® Materials Testing Software (Instron, Norwood, MA).

The femurs were positioned horizontally with anterior surface upwards, centered on the supports, and the pressing force was directed vertically to the mid-shaft of the bone. Each bone was loaded in anterior-posterior direction using an Instron 33R (Instron, Norwood, MA) at a rate of 0.2mm/s to a 40% decline in maximum load. All femoral samples were rotated to a similar position as visually checked.
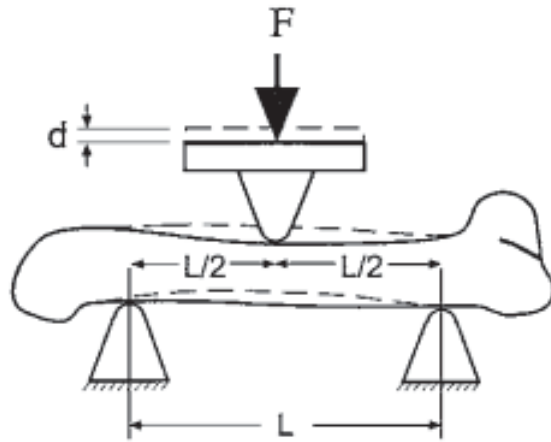
Figure 3-5.   Three-point bending test applied to mouse whole bone.
F is the applied force; d is the resulting displacement; and L is the span width.
(Reprinted with permission from Elsevier Science. Turner, C., & Burr, D. (1993). Basic
biomechanical measurements of bone: A tutorial. Bone, 14(4), 595-608.)

Statistical Methods

Mixed effects models were constructed to evaluate the association of strains with various bone properties, adjusted for the effects of gender and age. We used the Mixed Effects models because each strain was considered to be an independent cluster and measurements from mice within a strain were considered to be repeated measurements for that cluster. Association between femur and tibia in terms of a given bone property of interest was described using Spearman's rank correlation coefficient for each strain with at least 4 paired measurements. All analyses were conducted on SAS 9.3 (SAS Institute, Cary NC).

Mixed Effects Model

Mixed effects models are additive regression models that can handle correlated data. Regression analysis is commonly used to evaluate the relationship between variables, e.g. between a dependent variable and one or more independent variables. ANOVA is a form of regression analysis where the independent variable is a class variable with 2 or more levels. In regression models including one-way or two-way ANOVA, it is assumed that observations are independent of each other and the response variable follows a normal distribution. When the independence assumption is violated, the above approaches are no longer valid and more complex modeling strategies, such as mixed effects modeling, should be followed. In our data, measurements from multiple mice within a given strain are expected to be highly correlated due to identical genetic makeup within a strain, while strains themselves can be considered independent of each other.

As mentioned earlier, lab mice were raised under the same well-controlled condition, such as light exposure, food intake, living space, ambient temperature and physical activity. Given the elimination on those environmental factors, mice used on this project should be considered identical "twins" in the same strain. Thus, subjects used in the same strains could be considered repeated measures, which necessitate the use of mixed effects models to describe the association of strain with bone properties of interest.

Spearman's Rank Order Correlation

The Spearman's rank correlation coefficient is a non-parametric counterpart of Pearson's Correlation coefficient, to measure the linear association between two variables. It is because it doesn't require the normality of the variables as Pearson's correlation does.

This coefficient ranges from -1 (representing perfect negative rank correlation) to +1 (representing perfect positive rank correlation) between two variables, where 0 (zero) means no association was observed in terms of ranking. The sign of the Spearman

correlation indicates the direction of association between the two variables. When one variable tends to increase while the other variable decreases, the Spearman correlation coefficient would be negative, and vice versa.

CHAPTER 4.   RESULTS

The results from the Mixed Effects regression models and Spearman's rank correlation were presented below separately. A sample data was presented in **Table B-1** in **Appendix B**.

Mixed Effects Model

Mouse strain was significantly associated with all measured phenotypes after adjusting for gender and age except cortical bone volume fraction (**Table 4-1**). That is, the variation of quantitative bone features due to genetic variation would still be significant when both age and gender were included in the model.

From the table, we could tell that gender appeared to have a significant impact over most phenotypes as well. It meant that bone features of female and male appear to be largely different in the sample space. The direction of the influence was denoted in the parenthesis with "F-" representing female values smaller than male and "F+" indicating larger values in the females. Tibia and femur tended to be impacted by gender in the same orientation. For example, in mineralized volume, females tend to have smaller values than males in both femur and tibia ($p<0.0001$). However, it was not always true that quantitative phenotypes of long bones were smaller in females. For example, females inclined to have denser femur ($p=0.51$) than males. Also, the female presented higher trabecular SMI than males which indicated a more plate-like trabecular structures in female mice than males. These differences were therefore indicative of genetically based influence.

From the table, we observed most phenotypes did not show significant difference due to age disparity. Therefore, our concern about significant impact from age disparity became secondary.

Correlations

Spearman's rank correlation coefficients, indicating relationship between femurs and tibias, were presented in **Tables C-1** through **C-3** in **Appendix C**. These three tables illustrated the rank correlations for measurements taken on a level of whole bone, cortical and trabecular compartments, respectively.

Correlation across Strains

The existence of rank correlations varied from strain to strain. In whole bone profile, 16 strains showed strong association in cortical thickness between femur and tibia ($p<0.05$); while 2 were found with significant association in the bone mineral

Table 4-1.   **P-value of strain effect on bone morphological and biomechanical properties in femur and tibia of RI mice adjusted for gender and age (N>3).**

Measurement	Bone	Number of Strains	Percentage of Female	Age Range (week)	Strain	Gender	Age
Length	Femur	46	48.9	9.6-13.6	<0.0001	<0.0001(F-)	0.04(+)
	Tibia	46	52.0	9.6-13.6	<0.0001	0.075(F-)	0.23
mBMD	Femur	46	48.9	9.6-13.6	<0.0001	0.051(F+)	0.8
	Tibia	46	52.0	9.6-13.6	<0.0001	0.53	0.096(+)
Min. Vol	Femur	46	49.5	9.6-13.6	<0.0001	<0.0001(F-)	0.039(+)
	Tibia	46	52.0	9.6-13.6	<0.0001	<0.0001(F-)	0.35
Ct. Th	Femur	46	55.8	9.6-13.6	<0.0001	<0.0001(F-)	0.22
	Tibia	46	54.5	9.6-13.6	<0.0001	<0.0001(F-)	0.18
Ct. mBMD	Femur	46	55.8	9.6-13.6	<0.0001	0.014(F-)	0.86
	Tibia	46	54.5	9.6-13.6	<0.0001	0.02(F-)	0.09(+)
CSA	Femur	46	55.8	9.6-13.6	0.0048	<0.0001(F-)	0.59
	Tibia	46	54.5	9.6-13.6	0.01	0.0001(F-)	0.21
Ct. Ar	Femur	46	55.8	9.6-13.6	<0.0001	<0.0001(F-)	0.82
	Tibia	46	54.5	9.6-13.6	<0.0001	<0.0001(F-)	0.43
Trab. BV/TV	Femur	46	53.9	9.6-13.6	<0.0001	<0.0001(F-)	0.4
	Tibia	46	53.7	9.7-13.6	<0.0001	<0.0001(F-)	0.8
Conn. Dens	Femur	46	53.9	9.6-13.6	<0.0001	<0.0001(F-)	0.05(-)
	Tibia	46	53.7	9.7-13.6	<0.0001	<0.0001(F-)	0.087(-)
Trab. SMI	Femur	46	53.8	9.6-13.6	<0.0001	<0.0001(F+)	0.48
	Tibia	46	53.7	9.7-13.6	<0.0001	<0.0001(F+)	0.81
Trab. N	Femur	46	53.9	9.6-13.6	<0.0001	<0.0001(F-)	0.017(-)
	Tibia	46	53.7	9.7-13.6	<0.0001	<0.0001(F-)	0.25

Table 4-1.   (Cont'd).

Measurement	Bone	Number of Strains	Percentage of Female	Age Range (week)	Strain	Gender	Age
Trab. Th	Femur	46	53.9	9.6-13.6	<0.0001	<0.0001(F-)	0.87
	Tibia	46	53.7	9.7-13.6	<0.0001	<0.0001(F-)	0.01(+)
Trab. Sp	Femur	46	53.9	9.6-13.6	<0.0001	<0.0001(F+)	0.009(+)
	Tibia	46	53.7	9.7-13.6	<0.0001	<0.0001(F+)	0.35
Trab. mBMD	Femur	46	53.9	9.6-13.6	<0.0001	0.0007(F-)	0.23
	Tibia	46	53.7	9.7-13.6	<0.0001	0.018(F-)	0.65
Trab. DA	Femur	46	53.9	9.6-13.6	<0.0001	0.15	0.1(-)
	Tibia	46	53.7	9.7-13.6	<0.0001	0.08(F-)	0.91
Stiffness	Femur	46	54.0	9.7-13.6	<0.0001	0.0015(F-)	0.14
	Tibia	46					

P values no greater than 0.05 were highlighted in light grey and highlighted in dark grey if they were larger than 0.05 but less than 0.1.
F+ means females have higher values; F- means females have lower values.
(-) refers to negative association; (+) refers to positive association.

density at distal femur (**Tables C-1** through **C-3**). In the correlation of bone mineralized volume, BXD44 showed a perfect rank correlation between femur and tibia (p<0.0001) while BXD 95 was also observed to present the same correlation (p<0.0001); however, in the measurement of material bone mineral density, BXD44 was examined to reveal a negative correlation between femur and tibia (r=-0.4, p=0.6) while BXD95 presented an association of 0.9 (p=0.04).

Results were presented with strains with 4 or more paired measurements. Strains with only 3 paired samples or less are highly susceptible for significant correlation in Spearman's Rank Order Correlation analysis. There is no need to explain N=2 or 1. When N=3, there are simply 7 possible coefficients: +1, +0.87, +0.5, 0, -1, -0.87, -0.5.

In addition, the degrees of correlations between femur and tibia vary across strains. We observed positive correlation from 0.7 to 1 (in trabecular envelope) and negative correlation from -0.86 to -1 (in whole bone envelope). Even within the same bone phenotype, a variety of correlation coefficients were found across strains. For example, in trabecular thickness, BXD89 and BXD90 revealed significant correlations at 0.75 (p=0.05) and 0.7 (p=0.04) respectively, while BXD48 showed a significant correlation of 0.9 (p=0.04) as seen in **Figure 4-1**. This result showed that femur and tibia bone properties could relate to a various extent.

Moreover, there was a combination of positive and negative correlation observed in phenotypes across strains. The sign of the correlation coefficient (+ or -) represented the direction of association between femur and tibia. In positive relationships, the increasing of femoral values' ranks would be accompanied by ascending tibial phenotypic ranks; in negative relationships, the tibial phenotypes presented a reverse rank order when femoral features were ascending among subjects. For example, BXD1 and BXD80 mice with higher mineral density in femur tended to have denser tibias (r=1.0, p<0.0001 and r=0.76, p=0.03). However, BXD75 mice's tibias were less dense in those with higher mineral density in femur (r=-0.86, p=0.01) as shown in **Figure 4-2**.

Correlation within Strains

Variations in correlations were not only found across strains but also within strains. First of all, correlations were found in various combinations of phenotypes strain-wise. In whole bone profile, some strains showed significant femur-tibia correlation in all three measured phenotypes, including length, mineralized volume, and material bone mineral density (**Figure 4-3**); some strains showed significant long bone associations in two phenotypes (e.g. BXD60, and BXD62) and some revealed strong relationships in only one phenotypes (e.g. BXD80). In trabecular envelope, most strains had multiple phenotypes. For example, BXD89 revealed significant correlation in trabecular bone volume fraction (ρ=0.89, p=0.01), trabecular connectivity density (ρ=0.96, p<0.001), trabecular SMI (ρ=0.86, p=0.01), trabecular thickness (ρ=0.75, p=0.05), trabecular number (ρ=0.93, p<0.05) and trabecular space (ρ=0.93, p<0.05).
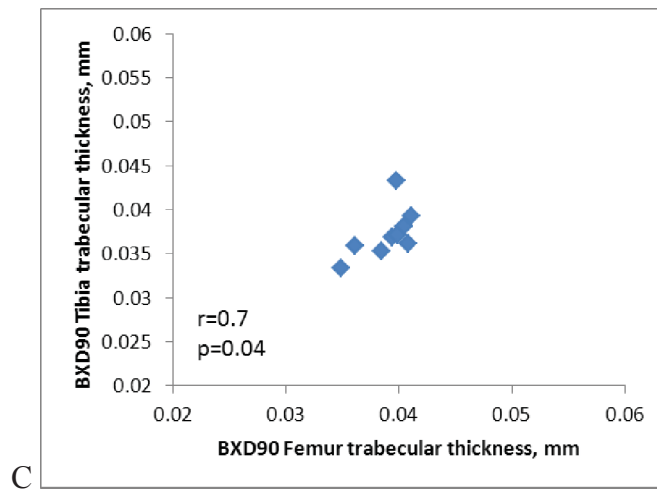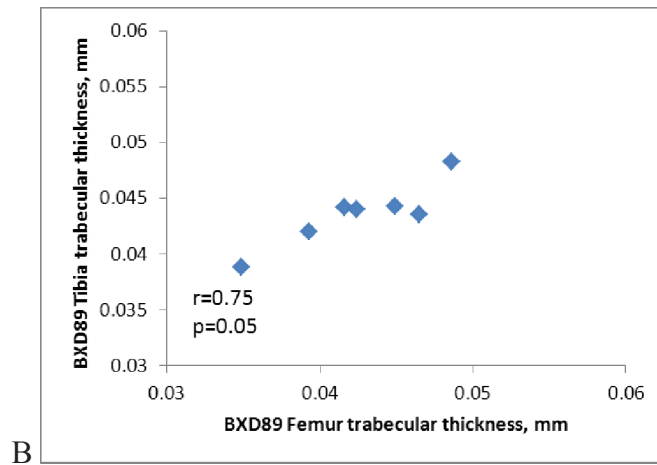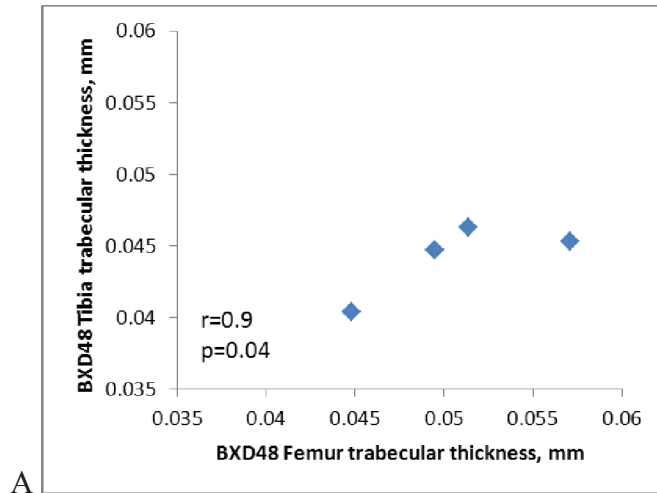
Figure 4-1. **Spearman's rank correlations in trabecular thickness showed strong positive association between femur and tibia.**
A) BXD48 (r=0.9, p=0.04); B) BXD89 (r=0.75, p=0.05); C) BXD90 (r=0.7, p=0.04).
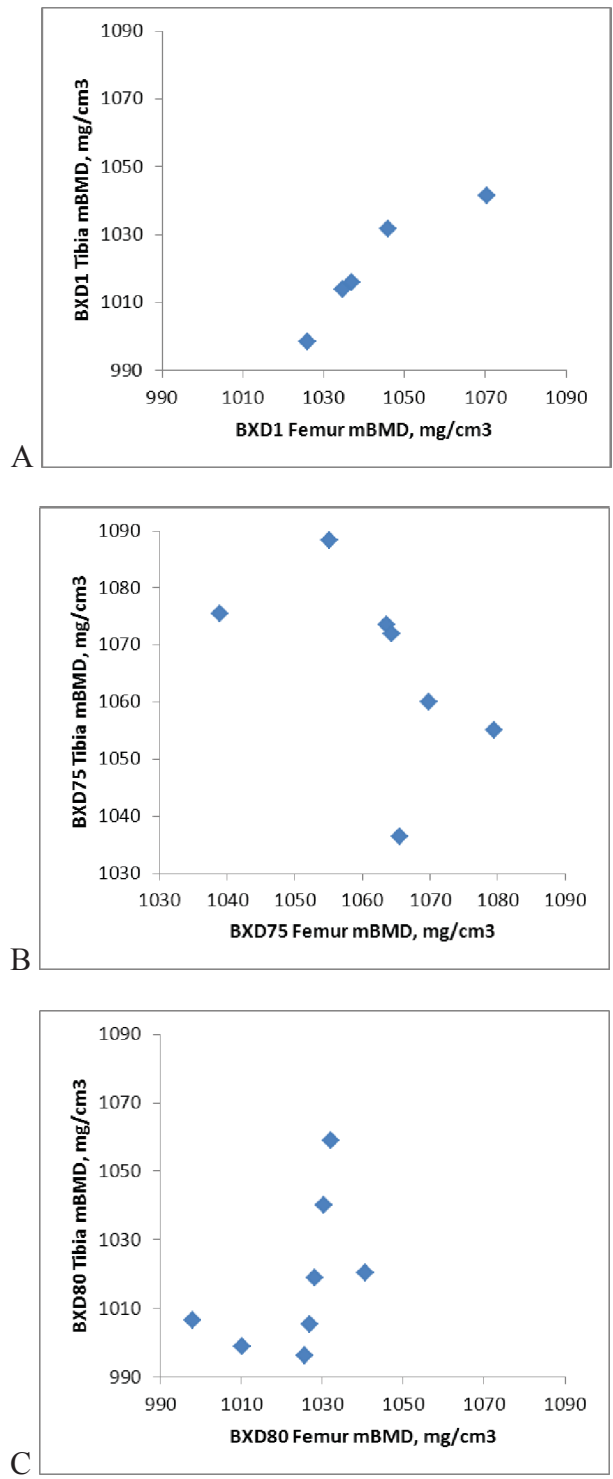
Figure 4-2. **Spearman's rank correlations in material bone mineral density differed between strains.**
A) BXD1 (r= 1.0, p<0.0001); B) BXD75 (r=-0.86, p=0.01); C) BXD80(r=0.9, p=0.04).
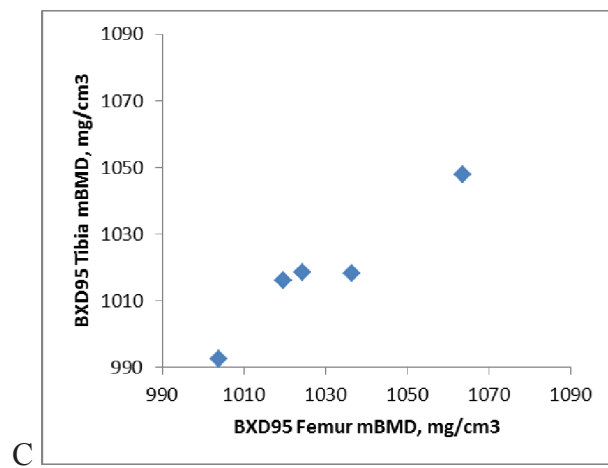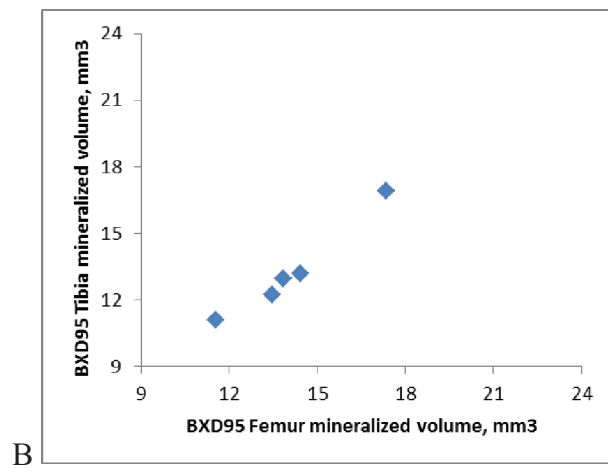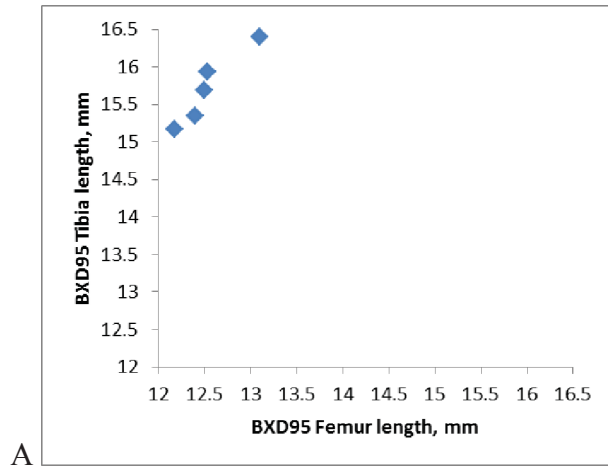
Figure 4-3.   Spearman's rank correlations in BXD95 whole bone profile showed a variety of association between femur and tibia.
A) r=1.0, p<0.0001; B) r=1.0, p<0.0001; C) r=0.9, p=0.04.

Secondly, a variety of correlations were observed within the same strains. Some bone features presented perfect ranking correlation (e.g. r=1) while some showed a smaller correlation. Take BXD89's trabecular profile for an example, femur-tibia correlation was found at 0.89 in trabecular bone volume ratio (p=0.01) while a stronger correlation (r=0.96, p<0.001) was discovered in the connectivity density. Similarly, different correlations were revealed in independent parameters, such as SMI (r=0.86, p=0.01), thickness (r=0.75, p=0.05), trabecular number (r=0.93, p<0.05).

Finally, in the same strain of mice, femur and tibia correlated in different directions indicated by the positive and negative associations derived across morphological parameters. For example, in both strain BXD1 and BXD100, femur and tibia correlated in a negative direction in cross-sectional area of the cortical bone (r=-0.90, p=0.04 and r=-0.89, p=0.02), while they were revealed with positive relationship in cortical bone area (r=0.9, p=0.04 and r=0.93, p=0.01). In another, in these two strains of mice, femurs with wider mid-shafts jointed with tibias with narrower mid-shaft, even though mice with thicker cortical bone in femur carried tibias with similar features.

CHAPTER 5. DISCUSSION

These data demonstrated for the first time in BXD mouse a genetic regulation in the correlation of femur and tibia. They also confirmed the previously reported genetic contribution to bone morphological and structural properties (Beamer et al., 1996; Turner et al., 2000; Turner et al., 2001; Bower et al., 2006). By phenotyping each BXD RI strain and the progenitor strains, analyses of resultant patterns yield insights about genetic regulation underlying each trait.

In summary, we came to the following conclusions:

i)   Differences were found in bone mass, morphological and micro-architectural properties across strains after controlling the effect of gender and age, e.g. whole mineralized volume;
ii) Differences were found in femoral stiffness across strains after controlling the effect of gender and age, e.g. stiffness;
iii) The degree of femur-tibia relationship along with the direction of association in bone morphology and micro-architecture was inferred to be genetically influenced.

The result supported our hypothesis that strain-wise bone property differences in addition to strain-wise correlation were present. The findings suggested that differences in the bone phenotypes (e.g. bone mass, bone morphology) were resulted from different combinations of gene segments passed on from the progenitor strains (B6 and D2). The living environment for those lab mice was well-controlled and identical. The significant differences observed in the quantitative characters of bones, comparing one strain to another, could be caused by the disparity between strains, that is, by different genetic makeup. What's more, significant differences were also shown in the stiffness indicating that it was highly influenced by genetic background as well.

The degree of femur-tibia correlation varies in both magnitude and direction. Femur and tibia's quantitative traits could change positively or negatively with each other, indicating that assessment of bone structure from femur couldn't be extrapolated to tibia without identifying related quantitative trait loci. This suggested finding, added to the investigation on genetic control on site-specific characters within a single bone (Judex, Garman, Squire, Donahue, & Rubin, 2004), illustrated that genetic influence played a role in various aspects of bone development.

Based on literature search in powerful scientific article search engine, such as Google Scholar and PubMed, no data have been published in relation to a possible genetic contribution to femur-tibia correlation in bone mass and bone micro-architecture. The exploration of the correlation should reveal fundamentally important process in the control of skeletal integrity.

Gender and Age Influence

Since these genetically distinct strains of mice were raised in a well-controlled environment (e.g. diet, living space), the differences observed in bone parameters are primarily expected to be the result of genetic variation.

Our results suggested that genetic factors played a role in cortical and trabecular strength and microstructure using long bones. Turner et al. reported genetic differences of cortical and trabecular micro-architecture in lumbar vertebrae (Turner et al., 2000). In our study, strain-specific differences were found in all measured morphological phenotypes, such as cortical and trabecular thickness ($p<0.0001$). Significant differences were also observed in mid-shaft stiffness.

Gender Difference

In the results, significant gender differences ($p<0.1$) were observed in all measured bone quantitative traits except in material bone mineral density in tibia and degree of anisotropy in femur. It is possible that some skeletal features of BXD RI mice at the age of 9.6 to 13.6 weeks are still undergoing active growth and female and male BXD mice tend to develop at a similar rate. Perhaps these two bone phenotypes develop in a slow process towards their peak.

For the observation that higher material bone mineral density was revealed in female ($p=0.051$), it is possible that, for BXD mice, females' active bone development is faster than male between 9.6- to 13.6-week. Normally, mice completed their puberty at the age of 10 weeks. However, both genetic and environmental factors (e.g. nutrition, stress) could alter the onset of puberty (Pinter, Beda, Csaba, & Gerendai, 2007). Alternatively, female long bone growth could be disproportionately greater, resulting noticeably different male and female skeletal density. Perhaps these recombinant inbred female mice have a unique combination of alleles that couples with sex genes to regulate bone development causing higher bone mineral density in females' femur at a later stage of puberty.

From the results, we observed that female RI mice were likely to have more rod-like trabecular structures ($p<0.0001$) along with wider space in between ($p<0.0001$) in the distal femur and proximal tibias. There was no significant difference found between female and male on the orientation of trabecular structure in femur while female tend to have less aligned trabeculae in tibia ($p=0.08$).

For biomechanical properties, gender-specific differences were observed as well. Smaller stiffness was found in females than males (**Table 4-1**). There were more females in the age of 12 week than males (about 15 more) while there are about 7 male mice at the age of 13 week but no females.

Age Influence

Positive association of age in multiple phenotypes (p<0.05), such as femoral length, femoral mineralized volume, femoral trabecular number and tibial trabeculcar thickness, indicated that these recombinant inbred mice at the age of 9.6 to 13.6 weeks were still experiencing a rapid bone development before reaching their peak bone mass stage. However, significant age influence was observed in 10 phenotypes (p<0.1) in either femur or tibia. For example, age had a higher association on femoral length (p=0.04) than tibia. It is possible that femur have longer bone development process and continues to grow while tibia has reached its peak status around the age of 13.6 week. Similar disparity was revealed in mineralized volume, trabecular number and trabecular space, indicative of longer femoral development process. As a special case, tibial trabecular thickness growth could be slow comparing with femur.

In addition, we observed declines in the connectivity density of both distal femur and proximal tibia for inbred mouse from the week of 9.6 to 13.6, confirmed with findings of Glatt et al. (2007). There seemed to be a decline in trabecular micro-architecture as age goes up comparing with previously published studies, such as bone volume ratio, bone mineral density, connectivity density, degree of anisotropy, trabecular number and thickness (**Table 5-1**). However, cortical bone appeared to be thickening during this process. It is possible that cortical bone continues to take major mechanical loading while trabecular bone would be reduced as a shielding effect.

Decline by age was also observed when comparing results with study from Bower et al (**Table 5-2**). Bower employed mice approximately 200 days old at the time of death (e.g. 28.6 weeks), when mice underwent aging and a series of degeneration in bone development.

Experimental Design

With further work, this dataset could be valuable for future genetic studies aimed at identifying the specific chromosomal regions and, ultimately, the specific sequence variants that contribute to bone morphological and structural properties.

Sample Collection and Storage

Mouse bone collection required considerable patience and techniques. The delicate mouse bones could be easily fractured and destroyed during surgery. This resulted in missing femoral heads or tibial ends in some bone specimens. Consequently, trabecular or whole bone data was not able to be consistently collected for all samples. Missing data requested our statistical analyses to be powerful. Therefore, the implementation of mixed model was required for data examination.

The best storage method for μCT was to seal specimens in 70% ethanol to

Table 5-1.   Femoral morphology measurements taken by micro-computed tomography for C57BL/6J RI mice.

Parameters	Martin et al. (2012)	Current Study		Judex et al. (2004)
Age (week)	5	10.7-11.7		16
Gender	Male	Male	Female	Female
Trabecular Bone Parameters				
Tb. BMD (mg HA/cm3)	149.9±11.3	116.8±63.4	74.5±53.7	
BV/TV	21.2±1.2	12.2±6.7	8.8±5.3	3.37±1.21
Tb. N	5.2±0.2	4.9±0.7	4.4±0.6	
Tb. Th (µm)	56.9±3.1	40.7±7.7	37.2±5.7	35.6±4.1
Tb. Sp (µm)	188.6±8.4	199.8±36.0	226.2±37.3	
Conn. Dens.	231.8±17.8	173.2±70.8	111.2±71.6	16.5±17.6
SMI	1.7±0.1	2.2±0.54	2.6±0.7	3.51±0.31
DA	1.89±0.05	1.63±0.12	1.6±0.16	1.26±0.08
Cortical Bone Parameters				
Ct. BMD	862.0±8.3	1027.0±26.6	997.6±51.3	
Ct. Th	146.2±7.3	0.21±0.03	0.19±0.03	
CSA	2.31±0.09	2.65±0.4	2.6±0.2	
Ct. Ar	0.60±0.03	0.85±0.12	0.74±0.1	

Sources: Martin, A., David, V., Li, H., Dai, B., Feng, J. Q., & Quarles, L. D. (2012). Overexpression of the DMP1 C-terminal fragment stimulates FGF23 and exacerbates the hypophosphatemic rickets phenoytype in Hyp mice. Molecular Endocrinology, 26(11) doi:10.1210/me/2012-1062.

Judex, S., Garman, R., Squire, M., Donahue, L., & Rubin, C. (2004). Genetically based influences on the site-specific regulation of trabecular and cortical bone morphology. Journal of Bone Mineral Research, 19(4), 600-606.

Table 5-2. **Phenotypic means ± SD for tibia in parental and BXD RI strains comparing measurements from Bower et al (2006).**

Strain	Trab BV/TV (%)		Trab Conn.Dens. (1/mm^3)		SMI	
	Current Study	Bower et al.	Current Study	Bower et al.	Current Study	Bower et al.
Female						
D2	13.3±2.3	3.03±2.23	138.08±33.1	3.96±6.32	2.06±0.13	2.69±0.36
B6	12.6±5.2	3.8±2.32	140.2±44.9	5.76±7.57	2.22±0.42	2.6±0.32
BXD14	9.0±1.2	4.19±2.89	149.9±34.8	9.26±7.51	2.64±0.32	2.92±0.63
BXD27	7.0±0.3	2.57±1.39	59.8±16.6	7.56±2.50	2.46±0.23	2.75±0.43
BXD32	18.2±2.5	5.9±2.88	213.6±10.2	16.44±11.88	1.75±0.29	2.34±0.38
Male						
B6	24.8±1.3	6.01±2.48	262.7±35.3	11.78±7.43	1.39±0.19	2.72±0.37
BXD11	19.2±7.5	12.46±3.97	241.9±64.1	35.93±10.61	1.83±0.69	2.33±0.38
BXD27	14.9±2.1	4.43±2.25	193.7±11.0	13.55±10.07	2.46±0.23	2.89±0.47
BXD29	18.1±1.0	5.07±1.5	259.4±35.1	12.83±3.28	1.83±0.69	2.56±0.22
BXD31	12.7±0.6	8.77±4.14	174.9±4.2	17.85±9.01	2.41±0.03	2.54±0.46
BXD32	16.5±5.1	8.35±2.71	241.1±45.8	26.68±16.51	1.76±0.42	2.69±0.37
BXD38	23.5±3.6	9.62±4.06	401.8±32.5	32.51±19.53	1.39±0.22	2.54±0.46

Source: Bower, A., Lang, D., Vogler, G., Vandenbergh, D., Blizard, D., Stout, J., Sharkey, N. (2006). QTL analysis of trabecular bone in BXD F2 and RI mice. Journal of Biomechanics, 21(8), 1267-1275. doi:10.1359/JBMR.060501.

preserve the mineralization. However, for mechanical testing, the best preparation method was to implement the experiments immediately after death or after storage in 10% neutral buffered formalin for 24 h. Even storage in formalin produced a 20% increase in bone hardness (Cowin, 2001). However, ethanol storage method for 100 days did not change the stiffness (Linde & Sorensen 1993), although alcohol tended to displace water with the bone matrix and thus tends to dry the bone (Cowin, 2001).

Most importantly, all samples were stored with the same method and the goal of this project was to identify the differences across strains that were resulted from genetic background, instead of quantifying the biomechanical properties of the specimens. Indeed, the strength of bone could be expected with higher values due to dryness. Nevertheless, the consistency of the experiment ensured the comparison between strains.

As a side note, best method for mechanical testing would be implemented immediately after animal death. Otherwise, PBS and freezing approach could outperform 70% ethanol in bone strength preservation.

Bone biomechanical properties vary with anatomical site and affected by the age and general health of the donor. In addition, the preparation and storage of bone specimens can affect the mechanical properties of the tissue. Important factors include specimen preservation, hydration, and temperature. For accurate results, researchers usually keep the specimens in physiological saline or wrapped with saline-soaked gauze during the test. However, it is found that drying-rehydration steps significantly reduced the bending strength. Therefore, the consistency of the experimental environment is more critical to the results.

Mechanical Testing

Cortical geometry was very influential on measurement of three-point bending. Observed from tibial micro-CT scans, tibial cross-sectional geometry at mid-shaft varied considerably. This consistence would largely contribute to the measurement error. Additionally, it did not fit in the criteria of the Timoshenko calculation (Schriefer et al., 2005). Errors due to local deformation of the specimen or ring deformation could be estimated using finite element analysis (FEA), where three-dimensional, orthotropic linear finite element model was established. However, FEA would be less feasible for project with a large number of specimens. Eventually, we chose to measure stiffness only on femurs only.

The difference in cortical thickness and cortical cross-sectional geometry is of clinical importance because cortical geometry (e.g. thickness of cortex and total bone width) was the primary determinants of bone strength. Males tended to be observed with thicker cortical shell.

On the side of fulcrums, two pieces of mounting clay were used to support heavy femoral heads for bones tending to rotate and land on its lateral surface (**Figure 5-1**).
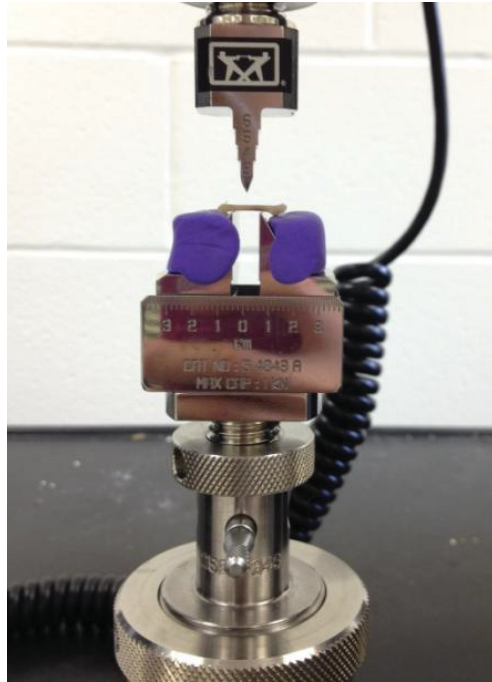
Figure 5-1. **Revised apparatus for three-point bending of RI mice long bones.**

μCT Measurement

Some measurements were not performed on imperfect sample that were severely damaged at measurement site. For example, length was not calculated from samples that presented a damaged proximal or distal site of the femur, while the measurements at mid-shaft were taken. This was a major reason for missing data case-wise.

As a tip for the imaging procedure, sample holders were covered with Parafilm® before immobilizing on the carousel inside the μCT chamber. The Parafilm® was used to prevent loss of moisture due to X-ray radiation for hours. For each sample holder, we also marked the sample ID on the outer wall of the tube with pencil to prevent sample holders mixed up.

Future Work

Some strains were eliminated from statistical analysis due to insufficient number of samples. Therefore, the immediate work in the future could be collecting samples and phenotyping available strains to extend the current BXD strain panel used in this project. In addition, it is possible to identify subgroups of BXD strains that possess similar bone phenotypes. This subgrouping could be integrated with a large database of genetic markers previously defined in the RI BXD strains to generate chromosome map a number of specific genetic loci, strongly related to lower limb quality.

In addition, we would apply the knowledge of BXD strains' bone phenotypes to identify related QTL, stretches of DNA containing or linked to the genes underlying a quantitative trait. Meanwhile, we could potentially identify subgroups of strains with similar bone phenotypes and identify pleiotropic QTL effects.

LIST OF REFERENCES

Airey, D., Lu, L., & Wlliams, R. (2001). Genetic control of the mouse cerebellum: Identification of quantitative trait loci modulating size and architecture. The Journal of Neuroscience, 21(14), 5099-5109.

Akhter, M., Iwaniec, U., Covey, M., Cullen, D., Kimmel, D., & Recker, R. (2000). Genetic variations in bone density, histomorphometry, and strength in mice. Calcified Tissue Int., 67, 337-344.

Arneson, T., Melton, L., & Lewallen, D. (1988). Epidemiology of diaphyseal and distal femoral fractures in Rochester, Minnesota. Clinical Orthopedic Related Research, , 188-194.

Beamer, W. G., Donahue, L. R., Rosen, C., & Baylink, D. (1996). Genetic variability in adult bone density among inbred strains of mice. Bone, 18(5), 397-403.

Bennett, B., Farber, C., Orozco, L., Kang, H., Ghazalpou, A., Siemers, N., Lusis, A. (2010). A high-resolution association mapping panel for the dissection of complex traits in mice. Genome Research, 20, 289-290.

Bower, A., Lang, D., Vogler, G., Vandenbergh, D., Blizard, D., Stout, J., Sharkey, N. (2006). QTL analysis of trabecular bone in BXD F2 and RI mice. Journal of Biomechanics, 21(8), 1267-1275. doi:10.1359/JBMR.060501

Chesler, E., Lu, L., Shou, S., Qu, Y., Gu, J., Wang, J., Williams, R. (2005). Complex trait analysis of gene expression uncovers polygenic and pleiotropic networks that modulate nervous systems function. Nature Genetics, 37, 233-242.

Cowin, S. C. (2001). In Cowin S. C. (Ed.), Bone biomechanics handbook (2nd ed.). U.S.: CRC Press LLC.

Cummings, S., Nevitt, M., & Browner, W. (1995). Risk factors for hip fractures in white women. New England Journal of Medicine, 332, 767-773.

Cunningham, C. L. (1995). Localization of genes influencing ethanol-induced conditioned place reference and locomotor activity in BXD recombinant inbred mice. Psychopharmacology, 120(1), 28.

Drake, T., Hannani, K., Kabo, J., Villa, V., Krass, K., & Lusis, A. (2001). Genetic loci influencing natural variations in femoral bone morphometry in mice. Journal Orthopedic Research, 19, 511-517.

Ferguson, V., Ayers, R., Bateman, T., & Simske, S. (2003). Bone development and age-related bone loss in male C57BL/6J mice. Bone, 33, 387-398.

Gaglani, S., Lu, L., Williams, R., & Rosen, G. (2009). The genetic control of neocortex volume and covariatin with neocortical gene expression in mice. BMC Neuroscience, 10(44), 1-11.

Gere, J., & Timoshenko, S. (1984). Mechanics of materials. Boston: PWS-Kent.

Glatt, V., Canalis, E., Stadmeyer, L., & Bouxsein, M. (2007). Age-related changes in trabecular architecture differ in female and male C57BL/6J mice. Journal of Bone Mineral Research, 22(8), 1197-1207.

Harrigan, T. P., & Mann, R. W. (1984). Characterization of microstructural anisotropy in orthotropic materials using a second rank tensor. Journal of Materials Science, 19(3), 761-767.

Hibderbran, T., & Ruegsegger, P. (1997). Quantification of bone microarchitecture with the structure model index. Cmbbe, 1, 15-23.

Hilderbrand, T., Laib, A., Muller, R., Dequeker, J., & Ruegsegger, P. (1999). Direct three-dimensional morphometric analysis of human cancellous bone: Microstructural data from spine, femur, illiac crest, and calcaneus. Journal of Bone Mineral Research, 14(7), 1167-1174.

Hilderbrand, T., & Ruegsegger, P. (1997). A new method for the model-independent assessment of thickness in three-dimensional images. Journal of Microscropy, 185, 67-75.

Hilderbrand, T., & Ruegsegger, P. (1997). Quantification of bone microarchitecture with the structure model index. Cmbbe, 1, 15-23.

Judex, S., Garman, R., Squire, M., Donahue, L., & Rubin, C. (2004). Genetically based influences on the site-specific regulation of trabecular and cortical bone morphology. Journal of Bone Mineral Research, 19(4), 600-606.

Kanis, J., Melton, L., Christiansen, C., Johnston, C., & Khaltaev, N. (1994). The diagnosis of osteoporosis. Journal of Bone Mineral Research, 9(8), 1137-1141.

Kiel, D., Zhang, Y., Hannan, M., Anderson, J., Baron, J., & Felson, D. (1996). The effect of smoking at different life stages on bone mineral density in elderly men and women. Osteoporosis International, 6, 240-248.

Klein, R., Mitchell, S., Phillips, T., Belknap, J., & Orwoll, E. (1998). Quantitative trait loci affecting peak bone mineral density in mice. Journal of Bone Mineral Research, 13(11), 1648-1656.

Klein, R., Turner, R., Skinner, L., Vartanian, K., Serang, M., Carlos, A., . . . Orwoll, E. S. (2002). Mapping quantitative trait loci that influence femoral cross-sectional area in mice. Journal of Bone Mineral Research, 17(10), 1752.

Krall, E., & Dawson-Hughes, B. (1993). Heritable and life-style determinants of bone mineral density. Journal of Bone Mineral Research, 8(1), 1-9.

Laitinen, K., & Valimaki, M. (1991). Alcohol and bone. Calcified Tissue International, 49(1), S70-S73.

Linde, F., & Sorensen, H. (1993). The effect of different storage methods on the mechanical properties of trabecular bone. Journal of Biomechanics, 26(10), 1249-1252.

Looker, A., Borrud, L., Dawson-Hughes, B., Shepherd, J., & Wright, N. (2012). Osteoporosis or low bone mass at the femur neck or lumbar spine in older adults: United states, 2005-2008. NCHS Data Brief, 93, 1-8.

Lu, L., Airey, D., & Williams, R. (2001). Complex trait analysis of the hippocampus: Mapping and biometric analysis of two novel gene loci with specific effects on hippocampal structure in mice. The Journal of Neuroscience, 21(10), 3503-3514.

Martin, A., David, V., Li, H., Dai, B., Feng, J. Q., & Quarles, L. D. (2012). Overexpression of the DMP1 C-terminal fragment stimulates FGF23 and exacerbates the hypophosphatemic rickets phenotype in Hyp mice. Molecular Endocrinology, 26(11) doi:10.1210/me/2012-1062

Martin, A., David, V., Vico, L., & Thomas, T. (2008). Impaired energetic metabolism after centeral leptin signaling leads to massive appendicular bone loss in hindlimb-suspended rats. Journal of Bone Mineral Research, 23(12), 2040-2047.

MicroCT intro-glossary. Retrieved from http://www.szsbetter.com/en/2-1.html

Muller, R. (1998). Morphometry. Retrieved from http://www.utc.fr/esb/esb98/abs_htm/MUELLER/morphometry.html. Accessed December 22, 2012.

Muller, R., & Reugsegger, P. (1997). Microtomographic imaging for the nondestructive evaluation of trabecular bone architecture. Studies of Health Technology Information, 40, 61-79.

Parfitt, A., Drezner, F., Glorieux, F. H., Kanis, J., Malluche, P., Meunier, S., & Recker, R. (1987). Bone histomorphometry standardization of nomenclature, symbols and units. Journal of Bone Mineral Research, 21, 595-610.

Peirce, J. L., Lu, L., Gu, J., Silver, L. M., & Williams, R. W. (2004). A new set of BXD recombinant inbred lines from advanced intercross populations in mice. BMC Genetics, 5(7), 1-17.

Pinter, O., Beda, Z., Csaba, Z., & Gerendai, I. (2007). Differences in the onset of puberty in selected inbred mouse strains. Endocrine Abstracts, 14, 617.

Pocock, N., Eisman, J., Hopper, J., Yeates, M., Sambrook, P., & Eberi, S. (1987). Genetic determinants of bone mass in adults. The American Society for Clinical Investigation, 80, 706-710.

Postnov, A., Vinogradov, A., Dyck, D., Saveliev, S., & Clerck, N. (2003). Quantitative analysis of bone mineral content by x-ray microtomography. Physiological Measurement, 24, 165-178.

Praemer, A., Furner S, & Rice, D. (1992). Musculoskeletal conditions in the United States. Park Ridge, IL: American Academy of Orthopedic Surgeons.

Schriefer, J., Robling, A., Warden, S., Fournier, A., Mason, J., & Turner, C. (2005). A comparison of mechanical properties derived from multiple skeletal sites in mice. Journal of Biomechanics, 38, 467-475.

Suwanwela, J., Farber, C., Haung, B., Song, B., Pan, C., Lyons, K., & Lusis, A. (2011). Systems genetics analysis of mouse chondrocyte differentiation. Journal of Bone Mineral Research, 26(4), 747-760.

Taylor, B., Wnek, C., Kotlus, B., Roemer, M., MacTaggart, T., & Phillips, S. (1999). Genotyping new BXD recombinant inbred mouse strains and comparison of BXD and consensus maps. Mammalian Genome, 10, 335-348.

Turner, C., & Burr, D. (1993). Basic biomechanical measurements of bone: A tutorial. Bone, 14(4), 595-608.

Turner, C., Hsieh, Y., Müller, R., Bouxsein, M., Baylink, D., Rosen, C., Beamer, W. (2000). Genetic regulation of cortical and trabecular bone strength and microstructure in inbred strains of mice. Journal of Bone Mineral Research, 15(6), 1126-1131.

Turner, C., Hsieh, Y., Müller, R., Bouxsein, M., Rosen, C., McCrann, M., & Donahue LR, B., WG. (2001). Variation in bone biomechanical properties, microstructure, and density in BXH recombinant inbred mice. Journal of Bone Mineral Research, 16(2), 206-213.

Twyman, R. (2002, August 28, 2002). Model organisms: The mouse. Message posted to http://genome.wellcome.ac.uk/doc_WTD020804.html. Accessed January 15, 2013.

Wade, C., & Daly, M. (2005). Genetic variation in laboratory mice. Nature Genetics, 37(11), 1175.

Whitehouse, W. (1974). The quantitative morphology of anisotropic trabecular bone. J Microscropy, 101(2), 153-168.

Willingham, M., Brodt, M., Lee, K., Stephens, A., Ye, J., & Silva, M. (2011). Age-related changes in bone structure and strength in female and male BALB/c mice. Calcified Tissue International, 86(6), 470-483.

APPENDIX A. PROTOCOL FOR HARVESTING MOUSE FEMUR AND TIBIA

MATERIALS AND REAGENTS
Inbred mice
CO2
70% ethanol
1.5 mL tubes
Sharp dissect scissor (sterile or sprayed with 70% ethanol)
Blunt end scissor (sterile or sprayed with 70% ethanol)
Start a 1st-level head or text here.

PROCEDURE
1. Immediately before surgery, sacrifice mice with CO2 asphyxiation followed by cervical dislocation.
2. Mice were then put on dissection board and sprayed with 70% ethanol
3. Remove fur and skin from legs by lifting skin at the base of each leg with tweezers and cutting away skin across thigh and down to ankle.
4. Using a blunt end scissor, making an incision 1 inch vertically from umbilical region to anterior region
5. Extend this incision along the medial aspect of both rear appendages
6. Peel skin down leg and over foot and firmly tug until it is removed.
7. Use a sharp scissor to remove muscle from entire leg so that bone is complete exposed.
8. Clean bones of any remaining muscle and place femur and tibia in 1.5 mL tubes respectively containing 70% EtHO.
9. Store tubes with specimens in room temperature for experiments.

APPENDIX B. SAMPLE DATA SET USED IN SAS

Table B-1.   Sample data set used in SAS programing with 10 strains of RI mice whole bone profile.

Animal Number	Strain	Sex	Age(days)	Femur Length (mm)	Femur Mineralized Volume (mm3)	Femur Material BMD (mg/cm3)
BXD1_f1	BXD1	F	71	12.279	14.4383	1070.385
BXD1_f2	BXD1	F	71	12.899	14.9652	1045.905
BXD1_M1	BXD1	M	85	12.765	18.4596	1034.704
BXD1_M2	BXD1	M	85	13.736	21.7461	1036.985
BXD1_M3	BXD1	M	85	13.364	18.9193	1025.986
BXD11_F1	BXD11	F	87	11.945	12.3451	1039.198
BXD11_F2	BXD11	F	87	12.3	13.1274	1018.139
BXD11_F4	BXD11	F	87	12.548	14.7955	1005.463
BXD11_M1	BXD11	M	76	12.283	15.9399	1030.613
BXD11_M2	BXD11	M	76	12.569	18.7779	1038.46
BXD11_m3	BXD11	M	76	12.327	16.6863	1032.759
BXD12_f1	BXD12	F	77	12.35	11.4639	1036.448
BXD12_f1	BXD12	F	84	12.389	10.8728	1061.733
BXD12_f2	BXD12	F	77			
BXD12_f2_Box6	BXD12	F	84	12.604	12.5431	1036.247
BXD12_f3	BXD12	F	84	12.315	11.3512	1056.971
BXD12_m1	BXD12	M	77	12.512	17.1509	1037.253
BXD12_m2	BXD12	M	77	11.975	11.3035	1017.669
BXD12_m3	BXD12	M	77	12.632	17.5974	1025.382
BXD12_m4	BXD12	M	77	12.639	16.76	1031.284
BXD14_f1	BXD14	F	80	12.148	11.7991	1016.261
BXD14_f2	BXD14	F	80	12.209	12.3018	1014.919
BXD14_f3	BXD14	F	80	12.328	11.7281	1031.619
BXD14_m1	BXD14	M	80	13.235	17.2758	1050.264
BXD14_m2	BXD14	M	80	12.875	13.711	1014.45
BXD14_m3	BXD14	M	80	12.729	12.552	1022.565
BXD14_m4	BXD14	M	80			
BXD24_f1	BXD24	F	85	12.089	12.2502	1053.886
BXD24_f2	BXD24	F	85			
BXD24_f3	BXD24	F	85	12.048	12.5051	1080.311

Table B-1.   (Cont'd).

Animal Number	Strain	Sex	Age (days)	Femur Length (mm)	Femur Mineralized Volume (mm3)	Femur Material BMD (mg/cm3)
BXD24_m1	BXD24	M	85	12.999	14.0357	1034.302
BXD24_m2	BXD24	M	85	12.841	14.9947	1086.146
BXD24_m3	BXD24	M	85			
BXD27_f1	BXD27	F	75	11.949	12.4237	1035.174
BXD27_f2	BXD27	F	75	12.107	11.6928	1029.205
BXD27_m1	BXD27	M	75	12.055	13.3013	1039.936
BXD27_m2	BXD27	M	73	11.579	13.1982	1052.41
BXD27_m3	BXD27	F	73	11.952	11.813	1045.167
BXD29_f1	BXD29	F	71			
BXD29_f2	BXD29	F	71	12.656	13.648	1034.906
BXD29_f3	BXD29	F	71			
BXD29_m1	BXD29	M	71	12.67	15.7347	1014.383
BXD29_m2	BXD29	M	71	12.432	14.7577	1012.035
BXD29_m3	BXD29	M	71	12.907	16.4828	1016.797
BXD31_f2	BXD31	F	73			
BXD31_m1	BXD31	M	73	12.17	14.0375	1046.441
BXD31_m2	BXD31	M	73	11.914	15.6968	1040.539
BXD31_m3	BXD31	M	73	11.978	15.3561	1058.447
BXD31_m4	BXD31	M	73	11.938	13.6347	1031.016
BXD32_f1	BXD32	F	80	12.024	13.9395	1072.732
BXD32_f2	BXD32	F	80	12.948	15.8681	1071.256
BXD32_f3	BXD32	F	80			
BXD32_f4	BXD32	F	80	12.401	14.2031	1051.337
BXD32_f5	BXD32	F	80	12.232	13.7276	1045.301
BXD32_m1	BXD32	M	80	12.574	14.8862	1068.507
BXD32_m2	BXD32	M	80	12.453	16.2688	1078.768
BXD32_m3	BXD32	M		12.676	15.4986	988.6286
BXD34_f1	BXD34	F	76	11.98	12.3765	1086.347
BXD34_f2	BXD34	F	76	12.062	11.6297	1077.427
BXD34_m1	BXD34	M	76	12.853	16.0697	1049.057

APPENDIX C. SUPPORTIVE TABLES FOR DATA ANALYSIS

Table C-1.   **Spearman's rank correlation coefficients and significance level of whole bone phenotypes between femur and tibia in RI mice (N>2).**

Strain	N	Length	Length (P-value)	Mineralized Volume	Mineralized Volume (P-value)	mBMD	mBMD (P-value)
B6D2	6	0.60	0.21	0.83	0.04	-0.09	0.87
BXD1	5	0.90	0.04	1.00	<0.0001	1.00	<0.0001
BXD100	7	-0.29	0.54	-0.11	0.82	0.25	0.59
BXD101	3	0.50	0.67	0.50	0.67	1.00	<0.0001
BXD102	6	-0.49	0.33	0.14	0.79	0.38	0.46
BXD103	2	NA	NA	NA	NA	NA	NA
BXD11	3	0.50	0.67	0.50	0.67	1.00	<0.0001
BXD12	5	-0.40	0.50	-0.10	0.50	0.30	0.62
BXD14	4	-0.60	0.40	0.20	0.80	0.80	0.20
BXD24	3	1.00	<0.0001	1.00	<0.0001	1.00	<0.0001
BXD27	5	0.10	0.87	0.80	0.10	-0.10	0.87
BXD29	4	0.40	0.60	0.80	0.20	0.60	0.40
BXD31	2	NA	NA	NA	NA	NA	NA
BXD32	7	-0.36	0.43	0.32	0.48	0.54	0.22
BXD34	3	0.50	0.67	0.50	0.67	-1.00	<0.0001
BXD38	2	NA	NA	NA	NA	NA	NA
BXD42	3	1.00	<0.0001	0.50	0.67	0.50	0.67
BXD44	4	1.00	<0.0001	1.00	<0.0001	-0.40	0.60
BXD45	2	NA	NA	NA	NA	NA	NA
BXD48	4	0.80	0.20	0.40	0.60	0.80	0.20

Table C-1.   (Cont'd).

Strain	N	Length	Length (P-value)	Mineralized Volume	Mineralized Volume (P-value)	mBMD	mBMD (P-value)
BXD49	4	0.80	0.20	0.80	0.20	-0.63	0.37
BXD50	5	0.90	0.04	1.00	<0.0001	0.60	0.29
BXD56	4	0.80	0.20	0.80	0.20	-0.40	0.60
BXD60	7	0.93	<0.01	1.00	<0.0001	0.46	0.29
BXD62	8	0.91	<0.01	0.83	0.01	0.48	0.23
BXD63	3	1.00	<0.0001	1.00	<0.0001	0.50	0.67
BXD68	4	1.00	<0.0001	1.00	<0.0001	-0.40	0.60
BXD69	4	0.80	0.20	0.80	0.20	0.40	0.60
BXD70	7	0.21	0.65	0.61	0.15	0.25	0.59
BXD71	6	-0.43	0.40	0.37	0.47	0.31	0.54
BXD73	2	NA	NA	NA	NA	NA	NA
BXD75	7	-0.21	0.65	-0.11	0.82	-0.86	0.01
BXD79	6	0.94	<0.01	0.94	<0.01	-0.43	0.40
BXD80	8	-0.16	0.71	0.60	0.12	0.76	0.03
BXD83	6	0.37	0.47	0.77	0.07	-0.66	0.16
BXD84	5	-0.80	0.10	-0.40	0.50	0.30	0.62
BXD85	3	0.50	0.67	1.00	<0.0001	1.00	<0.0001
BXD87	3	-1.00	<0.0001	0.50	0.67	-0.50	0.67
BXD89	6	0.71	0.11	0.94	<0.01	0.26	0.62
BXD90	9	0.90	<.001	0.78	0.01	0.65	0.06
BXD92A	5	0.30	0.62	0.50	0.39	0.40	0.50
BXD95	5	1.00	<0.0001	1.00	<0.0001	0.90	0.04
BXD97	4	0.40	0.60	-0.20	0.80	0.40	0.60

Table C-1.   (Cont'd).

Strain	N	Length	Length (P-value)	Mineralized Volume	Mineralized Volume (P-value)	mBMD	mBMD (P-value)
C57BL/6J	13	0.08	0.79	0.04	0.89	-0.13	0.67
D2B6F1	6	0.26	0.62	0.60	0.21	-0.26	0.62
DBA2J	10	-0.36	0.30	-0.49	0.15	-0.26	0.47

P values less than 0.05 and its variable values are highlighted with light grey.

Table C-2. Spearman's rank correlation coefficients and significance level of cortical bone phenotypes between femur and tibia in RI mice (N>2).

Strain	N	Ct. mBMD	Ct. mBMD (P-value)	Ct. Th	Ct. Th (P-value)	CSA	CSA (P-value)	Ct. Ar	Ct Ar (P-value)
B6D2	8	0.29	0.49	0.79	0.02	0.32	0.43	0.57	0.14
BXD1	5	-0.50	0.39	0.40	0.50	-0.90	0.04	0.90	0.04
BXD100	6	0.43	0.40	0.67	0.16	-0.89	0.02	0.93	0.01
BXD101	6	-0.60	0.21	-0.26	0.62	0.54	0.27	0.23	0.66
BXD102	6	-0.26	0.62	0.20	0.70	0.83	0.04	0.14	0.79
BXD103	3	0.50	0.67	0.50	0.67	0.50	0.67	0.50	0.67
BXD11	4	0.40	0.60	1.00	<0.0001	0.60	0.40	0.60	0.40
BXD12	5	-0.50	0.39	0.60	0.28	-0.30	0.62	0.10	0.87
BXD14	5	-0.80	0.10	0.00	1.00	-0.30	0.62	0.70	0.19
BXD24	5	-0.90	0.04	-0.60	0.28	0.30	0.62	0.70	0.19
BXD27	4	0.20	0.80	0.80	0.20	-1.00	<0.0001	1.00	<.0001
BXD29	4	-0.20	0.80	1.00	<0.0001	0.80	0.20	0.40	0.60
BXD31	2	NA	NA	NA	NA	NA	NA	NA	NA
BXD32	6	0.49	0.33	0.94	<0.01	0.14	0.79	0.46	0.35
BXD34	1	NA	NA	NA	NA	NA	NA	NA	NA
BXD38	4	0.40	0.60	-0.80	0.20	-1.00	<0.0001	0.20	0.80
BXD42	4	0.40	0.60	1.00	<0.0001	-1.00	<0.0001	-0.63	0.37
BXD44	7	0.04	0.94	0.89	0.01	0.68	0.09	0.82	0.02
BXD45	3	-0.50	0.67	1.00	<0.0001	-0.50	0.67	-0.50	0.67
BXD48	7	0.32	0.48	0.96	<0.001	0.80	0.02	0.89	0.01
BXD49	7	-0.50	0.25	0.75	0.05	0.71	0.07	0.96	<0.001
BXD50	5	0.50	0.39	1.00	<0.0001	-0.20	0.75	1.00	<0.0001

Table C-2.   (Cont'd).

Strain	N	Ct. mBMD	Ct. mBMD (P-value)	Ct. Th	Ct. Th (P-value)	CSA	CSA (P-value)	Ct. Ar	Ct Ar (P-value)
BXD56	5	0.40	0.50	0.90	0.04	0.90	0.04	0.82	0.09
BXD60	6	0.14	0.79	1.00	<0.0001	0.54	0.27	0.94	<0.01
BXD62	9	0.33	0.38	0.83	0.01	0.23	0.56	0.87	<0.01
BXD63	4	0.00	1.00	0.80	0.20	-0.20	0.80	0.40	0.60
BXD68	4	-0.32	0.68	-0.60	0.37	0.00	1.00	0.10	0.89
BXD69	6	-0.03	0.96	0.83	0.04	0.70	0.11	0.49	0.33
BXD70	7	0.46	0.29	0.60	0.15	-0.07	0.88	0.68	0.09
BXD71	7	-0.66	0.16	0.54	0.27	0.09	0.87	0.94	0.00
BXD73	5	1.00	<0.0001	0.00	1.00	0.00	1.00	0.00	1.00
BXD75	7	-0.29	0.53	0.64	0.12	-0.04	0.94	0.96	<0.001
BXD79	6	-0.54	0.27	0.94	<0.01	0.70	0.11	1.00	<0.0001
BXD80	9	-0.05	0.90	0.37	0.33	-0.55	0.13	0.47	0.21
BXD83	7	-0.36	0.43	0.25	0.59	0.27	0.55	0.46	0.29
BXD84	5	0.80	0.10	0.00	1.00	-0.30	0.62	-0.10	0.87
BXD85	3	1.00	<0.0001	1.00	<0.0001	0.50	0.67	1.00	<.0001
BXD87	5	0.90	0.04	0.60	0.28	0.70	0.19	0.70	0.19
BXD89	5	0.70	0.19	0.80	0.10	0.50	0.39	0.90	0.04
BXD90	9	0.37	0.33	0.82	0.01	0.43	0.24	0.83	0.01
BXD92A	5	-0.50	0.39	-0.10	0.87	-0.10	0.87	0.50	0.39
BXD95	5	0.90	0.04	0.70	0.19	0.70	0.19	0.70	0.19
BXD97	4	0.80	0.20	1.00	<0.0001	0.32	0.68	0.80	0.20
C57BL/6J	12	0.12	0.70	0.29	0.37	0.20	0.50	0.40	0.15
D2B6F1	6	0.14	0.79	0.94	<0.01	0.77	0.07	0.94	<0.01
DBA2J	11	-0.01	0.98	-0.06	0.85	-0.28	0.41	-0.18	0.59

P values less than 0.05 and its variable values are highlighted with light grey.

Table C-3. Spearman's rank correlation coefficients and significance level of cortical bone phenotypes between femur and tibia in RI mice (N>2).

Strain	N	Trab BV/TV	Trab BV/TV (P-value)	Trab Conn.Dens	Trab Conn.Dens (P-value)	Trab SMI	Trab SMI (P-value)	Trab Th	Trab Th (P-value)	Trab N	Trab N (P-value)	Trab Sp	Trab Sp (P-value)	Trab mBMD	Trab mBMD (P-value)
BXD1	4	0.80	0.20	0.20	0.80	1.00	<0.0001	0.80	0.20	0.20	0.80	0.20	0.80	0.80	0.20
BXD38	4	0.40	0.60	-0.40	0.60	0.40	0.60	1.00	<0.0001	-0.20	0.80	-0.20	0.80	0.80	0.20
BXD45	4	0.80	0.20	1.00	<0.0001	0.40	0.60	0.80	0.20	1.00	<0.0001	0.80	0.20	0.80	0.20
BXD69	4	1.00	<0.0001	0.80	0.20	1.00	<0.0001	0.80	0.20	0.60	0.40	0.80	2.00	0.40	0.60
BXD73	4	0.40	0.60	0.40	0.60	0.00	1.00	0.20	0.80	0.20	0.80	0.40	0.60	1.00	<0.0001
BXD84	4	-0.20	0.80	0.20	0.80	-0.40	0.60	0.60	0.40	-0.40	0.60	-0.40	0.60	0.40	0.60
BXD95	4	1.00	<0.0001	0.80	0.20	0.80	0.20	0.80	0.20	0.80	0.20	1.00	<0.0001	0.40	0.60
BXD97	4	0.40	0.60	0.40	0.60	-0.40	0.60	0.40	0.60	0.40	0.60	0.40	0.60	0.40	0.60
B6D2	5	0.60	0.28	0.30	0.62	0.50	0.39	0.80	0.10	0.60	0.28	0.50	0.39	0.60	0.28
BXD101	5	-0.10	0.87	0.60	0.28	-0.80	0.10	0.50	0.39	0.70	0.19	0.60	0.28	-0.80	0.10
BXD27	5	0.90	0.04	0.80	0.10	0.70	0.19	0.70	0.19	0.70	0.19	0.70	0.19	-0.40	0.50
BXD48	5	0.60	0.28	0.00	1.00	-0.50	0.39	0.90	0.04	0.00	1.00	0.00	1.00	-0.30	0.60
BXD49	5	0.90	0.04	1.00	<0.0001	0.90	0.04	0.30	0.62	1.00	<0.0001	1.00	<0.0001	0.40	0.50
BXD92A	5	0.05	0.90	-0.30	0.62	0.00	1.00	0.30	0.62	0.90	0.04	0.90	0.04	0.60	0.28
D2B6F1	5	0.50	0.39	0.60	0.62	0.50	0.39	0.00	1.00	0.20	0.74	0.20	0.75	0.60	0.28
BXD100	6	0.83	0.04	0.30	0.54	0.20	0.70	0.54	0.27	0.94	<0.05	0.89	0.02	0.14	0.79
BXD12	6	0.60	0.21	0.66	0.16	0.50	0.27	0.67	0.15	0.83	0.04	0.83	0.04	0.20	0.70
BXD62	6	0.71	0.11	0.89	0.02	0.83	0.04	0.03	0.96	0.83	0.04	0.77	0.07	0.60	0.21
BXD71	6	0.94	<0.05	0.43	0.40	0.54	0.27	-0.26	0.62	0.70	0.11	0.94	<0.01	0.60	0.21
BXD79	6	0.54	0.27	0.43	0.40	0.14	0.79	0.26	0.62	0.94	<0.05	0.89	0.02	0.66	0.16
BXD80	6	0.54	0.27	0.89	0.02	0.77	0.07	0.09	0.87	0.83	0.04	0.84	0.04	0.37	0.47
BXD102	7	-0.20	0.67	0.36	0.40	-0.07	0.88	-0.07	0.88	0.18	0.70	0.11	0.82	0.29	0.53
BXD32	7	0.82	0.02	0.43	0.34	0.89	0.01	0.54	0.22	0.54	0.22	0.46	0.29	-0.09	0.85

Table C-3.   (Cont'd).

Strain	N	Trab BV/TV	Trab BV/TV (P-value)	Trab Conn.Dens	Trab Conn.Dens (P-value)	Trab SMI	Trab SMI (P-value)	Trab Th	Trab Th (P-value)	Trab N	Trab N (P-value)	Trab Sp	Trab Sp (P-value)	Trab mBMD	Trab mBMD (P-value)
BXD60	7	0.79	0.04	0.64	0.12	0.86	0.01	0.74	0.06	0.64	0.12	0.64	0.12	0.79	0.04
BXD70	7	0.86	0.01	0.75	0.05	0.82	0.02	0.60	0.15	0.70	0.07	0.64	0.12	0.60	0.15
BXD83	7	0.36	0.43	0.68	0.09	0.57	0.18	0.07	0.88	0.68	0.09	0.68	0.09	0.25	0.59
BXD89	7	0.89	0.01	0.96	<0.001	0.86	0.01	0.75	0.05	0.93	<0.05	0.93	<0.05	0.00	1.00
C57BL/6J	8	0.36	0.39	0.17	0.69	-0.05	0.90	0.48	0.23	0.24	0.57	0.29	0.49	0.00	1.00
DBA2J	8	0.43	0.29	0.62	0.10	-0.17	0.69	0.31	0.45	0.52	0.18	0.64	0.09	0.24	0.57
BXD90	9	0.53	0.14	0.28	0.46	0.75	0.02	0.70	0.04	0.57	0.11	0.73	0.03	-0.20	0.59

P values less than 0.05 and its variable values are highlighted with light grey.

VITA

Yueying Angela Zhang was born 1987 in Hebei, China. She attended and graduated from the University of Nebraska-Lincoln in May 2010, with B.S. (Honors) in Biological Systems Engineering, minoring in Biomedical Engineering. In June 2010, she started to work as a research assistant at the University of Tennessee Health Science Center (UTHSC) and was enrolled as a Master student in August 2010. After she was admitted to the Biomedical Engineering and Imaging program at UTHSC, she joined Dr. Weikuan Gu's group and embarked on an exploration of bone properties in BXD mouse strains. In March 2013, she successfully defended her master thesis and she will be receiving her Master of Science in May 2013. In her spare time, she enjoys jogging, volleyball and reading.